

Evaluation of the Acoustic and Aerodynamic Characteristics of Several Slot-Baffle Configurations for Transonic Wind Tunnel Walls

J. L. Jacocks, D. W. Sinclair, and R. L. Parker, Jr.
ARO, Inc.

January 1981

Final Report for Period October 20 — November 15, 1978

Approved for public release; distribution unlimited.

**ARNOLD ENGINEERING DEVELOPMENT CENTER
ARNOLD AIR FORCE STATION, TENNESSEE
AIR FORCE SYSTEMS COMMAND
UNITED STATES AIR FORCE**

NOTICES

When U. S. Government drawings, specifications, or other data are used for any purpose other than a definitely related Government procurement operation, the Government thereby incurs no responsibility nor any obligation whatsoever, and the fact that the Government may have formulated, furnished, or in any way supplied the said drawings, specifications, or other data, is not to be regarded by implication or otherwise, or in any manner licensing the holder or any other person or corporation, or conveying any rights or permission to manufacture, use, or sell any patented invention that may in any way be related thereto.

Qualified users may obtain copies of this report from the Defense Technical Information Center.

References to named commercial products in this report are not to be considered in any sense as an indorsement of the product by the United States Air Force or the Government.

This report has been reviewed by the Office of Public Affairs (PA) and is releasable to the National Technical Information Service (NTIS). At NTIS, it will be available to the general public, including foreign nations.

APPROVAL STATEMENT

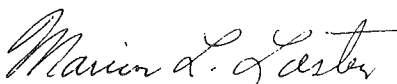
This report has been reviewed and approved.



ELTON R. THOMPSON
Project Manager
Directorate of Technology

Approved for publication:

FOR THE COMMANDER



MARION L. LASTER
Director of Technology
Deputy for Operations

UNCLASSIFIED

REPORT DOCUMENTATION PAGE		READ INSTRUCTIONS BEFORE COMPLETING FORM
1. REPORT NUMBER AEDC-TR-79-59	2. GOVT ACCESSION NO.	3. RECIPIENT'S CATALOG NUMBER
4. TITLE (and Subtitle) EVALUATION OF THE ACOUSTIC AND AERODYNAMIC CHARACTERISTICS OF SEVERAL SLOT-BAFFLE CONFIGURATIONS FOR TRANSONIC WIND TUNNEL WALLS	5. TYPE OF REPORT & PERIOD COVERED Final Report, October 20 - November 15, 1978	
	6. PERFORMING ORG. REPORT NUMBER	
7. AUTHOR(s) J. L. Jacocks, D. W. Sinclair, and R. L. Parker, Jr., ARO, Inc., a Sverdrup Corporation Company	8. CONTRACT OR GRANT NUMBER(s)	
9. PERFORMING ORGANIZATION NAME AND ADDRESS Arnold Engineering Development Center/DOT Air Force Systems Command Arnold Air Force Station, Tennessee 37389	10. PROGRAM ELEMENT, PROJECT, TASK AREA & WORK UNIT NUMBERS Program Element 921E07	
11. CONTROLLING OFFICE NAME AND ADDRESS Arnold Engineering Development Center/DOS Air Force Systems Command Arnold Air Force Station, Tennessee 37389	12. REPORT DATE January 1980	
	13. NUMBER OF PAGES 47	
14. MONITORING AGENCY NAME & ADDRESS (if different from Controlling Office)	15. SECURITY CLASS. (of this report) UNCLASSIFIED	
	15a. DECLASSIFICATION/DOWNGRADING SCHEDULE N/A	
16. DISTRIBUTION STATEMENT (of this Report) Approved for public release; distribution unlimited.		
17. DISTRIBUTION STATEMENT (of the abstract entered in Block 20, if different from Report)		
18. SUPPLEMENTARY NOTES Available in Defense Technical Information Center (DTIC).		
19. KEY WORDS (Continue on reverse side if necessary and identify by block number) wind tunnels acoustics transonic flow noise reduction ventilated walls wall characteristics baffles slots		
20. ABSTRACT (Continue on reverse side if necessary and identify by block number) An experimental investigation was conducted to record the acoustic and aerodynamic performance of several slotted walls with transverse baffles in the slots for transonic test sections. Primary configuration variables were the baffle angle inclination relative to the airstream and a wire mesh screen on the airside wall surface. At all baffle angles, the addition of the screen overlay decreased the acoustic noise level and improved the flow generation		

UNCLASSIFIED

UNCLASSIFIED

20. ABSTRACT, Concluded.

and supersonic wave cancellation properties of the wall but increased the subsonic wall interference effects.

UNCLASSIFIED

PREFACE

The work reported herein was performed by the Arnold Engineering Development Center (AEDC), Air Force Systems Command (AFSC) for the National Aeronautics and Space Administration (NASA), Ames Research Center, Moffett Field, California. The NASA project manager was Mr. F. W. Steinle, Jr. The experimental results presented were obtained by ARO, Inc., AEDC Division (a Sverdrup Corporation Company), operating contractor for the AEDC, AFSC, Arnold Air Force Station, Tennessee, under ARO Project Number P34A-W4. The Air Force project managers were Mr. A. F. Money and Mr. E. R. Thompson, AEDC/DOTR. The manuscript was submitted for publication on July 17, 1979.

CONTENTS

	<u>Page</u>
1.0 INTRODUCTION	5
2.0 APPARATUS	
2.1 Acoustic Research Tunnel	5
2.2 Aerodynamic Wind Tunnel	6
2.3 Wall Samples	7
3.0 PROCEDURE	
3.1 Acoustic Tests	7
3.2 Aerodynamic Tests	8
3.3 Wall Characteristics Evaluation	9
3.4 Precision of Results	11
4.0 RESULTS AND DISCUSSION	
4.1 Acoustic Characteristics	11
4.2 Flow Generation	13
4.3 Wave Cancellation	13
4.4 Wall Characteristics	14
5.0 CONCLUDING REMARKS	14
REFERENCES	15

ILLUSTRATIONS

Figure

1. Acoustic Research Tunnel Test Section Arrangement	17
2. Wall Sample Dimensions	18
3. Baffle Geometry	19
4. Top and Bottom Wall Samples for the Acoustic Research Tunnel	20
5. Tunnel Pressure Ratio Schedule for Tunnel 1T	21
6. Reynolds Number Envelope for Tunnel 1T	22
7. Spectra and Overall Noise Level at Zero Baffle Angle	23
8. Spectra and Overall Noise Level at 15-deg Baffle Angle	24
9. Spectra and Overall Noise Level at 30-deg Baffle Angle	26
10. Spectra and Overall Noise Level at 45-deg Baffle Angle	27
11. Effect of Screen Overlay on the Noise Spectrum	28
12. Effect of Baffle Angle on the Overall Noise Level	29
13. Representative Centerline Static Pressure Distributions	30

14. Effect of Wall Angle on the Centerline Static Pressure Distribution, $\phi = 0$, $M_c = 0.8$, Screen Off	32
15. Effect of Wall Configuration on the Centerline Static Pressure Distribution, $M_c = 1.2$	33
16. Effect of Wall Configuration on the Flow Uniformity Figure of Merit	34
17. Effect of Wall Configuration on the Tunnel Calibration Parameter	36
18. Representative Wedge Static Pressure Distributions	37
19. Effect of Wall Configuration on the Wedge Static Pressure Distribution, $M_c = 1.2$	39
20. Effect of Wall Configuration on the Wave Cancellation Figure of Merit	40
21. Representative Flow Angle and Static Pressure Distributions at the Ventilated Wall, $M_c = 0.8$	41
22. Effect of Screen Overlay and Mach Number on the Wall Characteristic, $\phi = 45$ deg	44
23. Effect of Wall Configuration on the Wall Interference Alleviation Figure of Merit	45

TABLE

1. Test Configurations	46
NOMENCLATURE	47

1.0 INTRODUCTION

The existing wall configuration of the National Aeronautics and Space Administration (NASA) 11- by 11-ft and 14- by 14-ft transonic tunnels consists of longitudinal slots with transverse baffles which are a source of discrete frequency acoustic noise of high intensity (Refs. 1 and 2).

In the search for a possible improvement to slot geometry that would eliminate the noise and improve the wall interference characteristic, a preliminary study was undertaken at the Arnold Engineering Development Center (AEDC) in the Acoustic Research Tunnel (ART) to determine effects of the baffle inclination angle, depth, and shape. That study concluded that a combination of 45-deg baffle inclination with a wire screen mesh overlay on the airstream side of the tunnel wall would be effective in reducing the noise levels. However, the slot size selected for the investigation was not scaled with respect to wall boundary-layer thickness or tunnel size.

The present study was conducted to investigate and verify the noise reduction with properly scaled hardware and to identify the aerodynamic characteristics of the baffle-slot with respect to a) flow generation and wave cancellation properties and b) subsonic wall interference alleviation capabilities. Tests were conducted in the Acoustic Research Tunnel and the Aerodynamic Wind Tunnel (1T) for six baffle inclination angles with and without screen overlays at Mach numbers from 0.2 to 1.4.

2.0 APPARATUS

2.1 ACOUSTIC RESEARCH TUNNEL

The Acoustic Research Tunnel (ART) is an open-circuit atmospheric indraft tunnel that operates on the plenum evacuation system (PES) of the 16-ft Transonic Tunnel (16T). The ART is capable of operation over the Mach number range from 0.10 to 1.10. Ventilated test section walls, wall divergence, and plenum suction are required at Mach numbers above 0.7.

The standard configuration of the ART consists of a converging nozzle with a contraction ratio of 16, a 6-in.-square by 24-in.-long test section, and a 5-deg diffuser. The ART was designed for the study of the acoustic characteristics of transonic wind tunnel walls. Therefore, mechanical vibration isolation joints and acoustic mufflers were installed in the exhaust line to minimize disturbances originating in the tunnel compressors. A honeycomb and a fine mesh screen are used in the stilling chamber to provide a uniform flow in the test section. Further details concerning the ART can be found in Ref. 3.

The basic instrumentation for the acoustic tests performed in the ART consisted of a pressure measurement system, a sidewall microphone, and a spectrum analyzer.

The pressure measurement system used a 15-psid strain-gage transducer to convert tunnel pressures to a d-c voltage signal. The output of the transducer was displayed on a digital voltmeter. The tunnel pressures were connected to the transducer via two 12-port scanning valves. The principal pressures measured during the acoustic tests were the tunnel total pressure, tunnel static pressure, and plenum pressure. Tunnel static pressures were measured at 1-in. intervals along the sidewall of the test section. The orifice located 1.5 in. upstream of the microphone (as shown in Fig. 1) was used as a reference to set tunnel flow conditions.

A 0.25-in.-diam Bruel & Kjaer® Model 4136 condenser microphone was used to measure the tunnel sound pressure level. The microphone was flush mounted to the sidewall of the test section at station 17.5 in., as shown in Fig. 1. The output of the microphone was displayed on a Hewlett-Packard® RMS digital voltmeter. A frequency analysis was performed on the microphone output at each operating condition using a real-time Fourier spectrum analyzer with 32 ensemble averages. Sharp peaks in the spectra were identified and then recorded with Polaroid® photographs.

2.2 AERODYNAMIC WIND TUNNEL

The AEDC Aerodynamic Wind Tunnel (1T) is a continuous flow, nonreturn wind tunnel equipped with a two-dimensional nozzle and an auxiliary plenum evacuation system. The Mach number range is from 0.2 to 1.5; variable nozzle contours are used at and above $M_\infty = 1.1$. The tunnel total pressure is nominally 2,850 psfa. The stagnation temperature is varied from 80 to 120°F above ambient temperature as necessary to prevent occurrence of visible condensation.

The test section is composed of four removable walls for a test region 37.5 in. in length and 12 by 12 in. in cross section. The top and bottom walls are supported by flexures at the nozzle exit and screw actuators at the downstream end to allow variations in wall angle. For this investigation, the tunnel was converted to a two-dimensional configuration by incorporating solid sidewalls, one of which had longitudinal lines of static pressure orifices on the centerline (2-in. spacing) and 5 in. above the centerline (1-in. spacing). Vertical lines of pressure orifices (1-in. spacing) were located at tunnel stations 1 and 32. (Tunnel station refers to the distance in inches from the nozzle exit).

Three distinct test section arrangements were utilized: (1) baffle-slot ventilated specimens as the top wall (see Section 2.3) for documentation of the flow generation properties with a

flat bottom wall; (2) a baffle-slot top wall with a 2-deg wedge plate as the bottom wall for documentation of the supersonic wave cancellation properties; and (3) a baffle-slot top wall with a contoured bottom wall for documentation of the basic subsonic wall characteristics.

The plenum chamber reference pressure, tunnel total pressure, and diffuser exit pressures were measured by 15-psid strain-gage transducers. Wall static pressures were measured by 15-psid strain-gage transducers using five modular 48-port Scanivalves®. The tunnel total temperature was measured by an iron-constantan thermocouple. The instrumentation readings were recorded by an online computer system which reduced the raw data to engineering units, computed pertinent parameters, and tabulated the results. The raw data were also recorded on punched paper tape for subsequent processing on the AEDC central computer system.

2.3 WALL SAMPLES

The slotted walls in the NASA/Ames transonic tunnels are formed by 10-in. structural steel channels laid side by side with a gap of 0.625 in. between the flanges. The dimensions of scaled channels of the top and bottom wall inserts for ART are given in Fig. 2 with the various baffle angles as shown in Fig. 3. The upstream end of the baffle-slot was partially covered with a tapered strip to provide a smooth transition from the nozzle exit as illustrated in Fig. 4. The walls utilized in Tunnel 1T had four slots with the same slot spacing, beginning at tunnel station 2. The screen overlay used in both tunnels was 40 by 60 mesh with 0.0065-in. wire diameter. The configuration combinations tested during each phase are noted in Table 1. Two baffle depths (shallow and deep) were evaluated at a baffle angle of 15 deg as noted in Table 1 and Fig. 2.

3.0 PROCEDURE

3.1 ACOUSTIC TESTS

Prior to each run, the condenser microphone was calibrated in situ by application of a 140-db sound pressure level at a frequency of 1 kHz. The piston phone used for calibration had a certified accuracy of ± 0.5 db. The spectrum analyzer was calibrated using an internally generated signal according to procedures supplied by the manufacturer.

Test conditions were established using standard ART procedures. Data were acquired at Mach numbers from 0.2 to 0.85.

Performance levels of each wall configuration were quantified using the integrated root-mean-square fluctuating pressure normalized by the test section dynamic pressure as a figure of merit, expressed as a percentage.

3.2 AERODYNAMIC TESTS

Although the operating characteristics of transonic wind tunnels are dependent on the ventilated wall geometry, this test used standard Tunnel 1T procedures for setting test conditions. The nominal Mach number was defined on the basis of an isentropic expansion from the tunnel total pressure to the plenum chamber pressure, and the total pressure ratio across the test leg, λ , was varied as a function of the Mach number according to the schedule given in Fig. 5. The result of this procedure is that the Mach number in the test section differs from the nominal Mach number dependent on wall geometry. Moreover, longitudinal gradients in Mach number at the rear of the test section were also wall dependent. However, this test procedure allowed direct comparisons of the ventilated wall characteristics.

The data were acquired at discrete plenum Mach numbers as listed below:

<u>Test Phase</u>	<u>Mach Number</u>
Flow Generation	0.6 to 1.4
Wave Cancellation	0.8 to 1.3
Wall Characteristics	0.5 to 0.9

The corresponding range of Reynolds numbers is given in Fig. 6.

For the flow generation phase, the static pressure on the tunnel sidewall centerline was selected as the primary indicator of longitudinal flow uniformity, and a figure of merit was defined as

$$\Delta M_{\text{L}} = 2 \left[\frac{1}{14} \sum_{I=1}^{14} M_I^2 - \left(\frac{1}{14} \sum_{I=1}^{14} M_I \right)^2 \right]^{\frac{1}{2}} \quad (1)$$

The summations extended from tunnel stations 10 to 30.

For the wave cancellation phase, the static pressures downstream of the wedge shoulder were used as the primary indicator of the wave cancellation characteristic of the ventilated wall, and a figure of merit was defined as

$$\Delta M_{\text{w}} = 2 \left[\frac{1}{37} \sum_{I=1}^{37} M_I^2 - \left(\frac{1}{37} \sum_{I=1}^{37} M_I \right)^2 \right]^{\frac{1}{2}} \quad (2)$$

where the summations extended from tunnel stations 13 to 35.

3.3 WALL CHARACTERISTICS EVALUATION

The performance of ventilated walls has conventionally been presented as the locus of local pressure coefficient versus local flow angle and has been termed the wall characteristic. A method of evaluating this characteristic without measurement of flow angles is given in Ref. 4 and is the basis for the present study. Briefly, the technique consists of the following procedure:

1. Experimentally establish two-dimensional flow between a ventilated wall sample and a contoured solid wall;
2. Measure the static pressure distributions at convenient upstream and downstream locations, on the contoured wall, and along a streamwise line in the vicinity of the ventilated wall;
3. Using the measured pressures as boundary conditions, solve for the interior flow field compatible with the transonic, two-dimensional, small perturbation potential equation as follows:

$$\left[1 - M^2 - (\gamma + 1) M^2 \Phi_x \right] \Phi_{xx} + \Phi_{yy} = 0 \quad (3)$$

4. Compute the flow angle distribution in the vicinity of the ventilated wall as follows:

$$\theta_T(x, h) = \Phi_y(x, h) \quad (4)$$

Given the measured static pressure distribution $C_{pT}(x, h)$ and the inferred flow angle distribution $\theta_T(x, h)$, it is possible to compute the distribution of these parameters which would exist in an environment free of wall interference — the desired wall characteristic — using the one-step adaptive wall equations of Lo and Kraft (Ref. 5). These relations may be written as

$$\begin{aligned} C_{p_{IF}}(x, h) = & \frac{1}{2} C_{pT}(x, h) - \frac{\beta h}{\pi} \int_{-\infty}^{\infty} \frac{C_{pT}(\xi, h) d\xi}{(2\beta h)^2 + (\xi - x)^2} \\ & + \frac{1}{\pi\beta} \int_{-\infty}^{\infty} \frac{\theta_T(\xi, h) (\xi - x) d\xi}{(2\beta h)^2 + (\xi - x)^2} + \frac{1}{\pi\beta} \int_{-\infty}^{\infty} \frac{\theta_T(\xi, h) d\xi}{\xi - x} \end{aligned} \quad (5)$$

$$\begin{aligned}
\theta_{IF}(x, h) = & \frac{1}{2} \theta_T(x, h) + \frac{\beta h}{\pi} \int_{-\infty}^{\infty} \frac{\theta_T(\xi, h) d\xi}{(2\beta h)^2 + (\xi - x)^2} \\
& + \frac{\beta}{4\pi} \int_{-\infty}^{\infty} \frac{C_{pT}(\xi, h) (\xi - x) d\xi}{(2\beta h)^2 + (\xi - x)^2} - \frac{\beta}{4\pi} \int_{-\infty}^{\infty} \frac{C_{pT}(\xi, h) d\xi}{x - \xi}
\end{aligned} \tag{6}$$

These integrals were numerically evaluated with extrapolation of the tunnel values to upstream-downstream infinity assumed to be exponential decay from the measurement end points. Examination of other means of extrapolation showed the results to be reasonably independent of the method of extrapolation. It should be noted that the C_p - θ locus for interference-free flow is not unique but is weakly affected by the effective contour of the bottom wall as influenced by wall interference.

To quantify the deviation of the measured characteristic from the desired characteristic, a figure of merit was constructed as

$$\Delta(C_p, \theta) = \Gamma_3 + 4\Gamma_6$$

where

$$\Gamma_3^2 = \Gamma_1^2 - \Gamma_2^2$$

$$\Gamma_6^2 = \Gamma_4^2 - \Gamma_5^2$$

$$\Gamma_1^2 = \frac{1}{31} \int_{x=1}^{32} \left(C_{pT} - C_{pIF} \right)^2 dx$$

$$\Gamma_2 = \frac{1}{31} \int_{x=1}^{32} \left(C_{pT} - C_{pIF} \right) dx$$

$$\Gamma_4^2 = \frac{1}{31} \int_{x=1}^{32} \left(\theta_T - \theta_{IF} \right)^2 dx$$

$$\Gamma_5 = \frac{1}{31} \int_{x=1}^{32} \left(\theta_T - \theta_{IF} \right) dx$$

Note that the flow angle deviation is weighted by a factor of four to yield a magnitude comparable to the pressure coefficient deviation.

3.4 PRECISION OF RESULTS

The uncertainties (combinations of systematic and random errors) of the basic tunnel parameters were established from repeat calibration of the instrumentation and from the repeatability and uniformity of the test section flow during tunnel calibration. Uncertainties in the instrumentation systems were estimated from repeat calibration of the systems against secondary standards whose uncertainties are traceable to the National Bureau of Standards calibration equipment. The instrument uncertainties were combined using the Taylor series method of error propagation.

The uncertainties in the results are given below.

C_p	± 0.006	M_∞	± 0.005	ΔM_{CL}	± 0.0013
M_c	± 0.005	$\Delta C_{p_{rms}}$	± 0.2	ΔM_w	± 0.0008
$M_{CL} - M_c$	± 0.002	$\Delta(C_p, \theta)$	± 0.003	θ	± 0.002

4.0 RESULTS AND DISCUSSION

4.1 ACOUSTIC CHARACTERISTICS

Data were obtained through the Mach number range from 0.2 to 0.85 to evaluate the acoustic characteristics of various slot-baffle angles. Measurements included the overall test section sound pressure level and the detailed frequency content of the noise. Each baffle angle configuration was evaluated with and without a wire mesh overlay.

4.1.1 0-deg (Normal) Baffle

The acoustic characteristics of the 0-deg (normal) baffle are shown in Fig. 7. The noise spectra at several Mach numbers are shown in Fig. 7a. The test section noise content is predominantly broad band with only a weak, wall-induced, discrete spike at approximately 16 kHz at Mach numbers from 0.8 to 0.7. Note that the relative amplitudes of the spectra are not comparable between different Mach numbers because of the use of different gain settings on the analyzer. The sound pressure level, Fig. 7b, increases monotonically through the Mach number range 0.2 to 0.85 with a fluctuating pressure coefficient ($\Delta C_{p_{rms}}$) variation from 0.8 to 1.2 percent. Also shown in Fig. 7b are the measured $\Delta C_{p_{rms}}$ values for a solid wall test section and the 0-deg baffle configuration with a wire mesh overlay. The wire mesh attenuated the noise and yielded a sound pressure level slightly below that for the solid wall.

4.1.2 15-deg Baffle

Both shallow and deep 15-deg baffle configurations were evaluated, and their characteristics are shown in Fig. 8. The noise spectra for the shallow baffle (Fig. 8a) indicate a weak discrete frequency spike at 16 kHz at Mach numbers below 0.5. There is a large magnitude discrete frequency, wall-induced tone at approximately 9 kHz at Mach number 0.5 as well as large low frequency disturbance at Mach number 0.85. (These large acoustic disturbances are also illustrated in Fig. 8c, which shows a significant increase in the sound pressure level.) The noise spectra for the deep baffle (Fig. 8b) contained discrete frequency spikes at 8.4 and 16 kHz at Mach numbers above 0.4. The peaks for the deep baffle were not as large near Mach number 0.5 as were those for the shallow baffle, as Fig. 8c shows; however, they were sufficiently large to cause the sound pressure level to exceed that for the shallow baffle at Mach number 0.6 and above. The screen overlay was effective in suppressing the wall-generated noise, yielding the same sound pressure levels for both configurations, as indicated in Fig. 8c.

4.1.3 30-deg Baffle

The acoustic characteristics of the 30-deg baffle configuration are shown in Fig. 9. The frequency content of the test section noise (Fig. 9a) is dominated by relatively broadband, low-frequency energy, which is generally associated with a wall/plenum-coupled resonance phenomenon. The sound pressure level is shown in Fig. 9b. Although there are no significant resonant peaks as with the 15-deg shallow baffle, the overall sound pressure level is higher than that for the baffle configurations of smaller angles.

The wire mesh overlay was effective in suppressing the noise generation of the wall, Fig. 9b. As with the other configurations, the sound pressure level with the overlay is reduced to a value slightly below the solid wall reference configuration.

4.1.4 45-deg Baffle

The acoustic characteristics of the 45-deg baffle configuration are shown in Fig. 10. As with the 30-deg baffle, the frequency content of the test section noise is predominantly broadband, low-frequency energy (Fig. 10a). The magnitude of the low-frequency noise is sufficiently large to cause the sound pressure level to be larger than that for the smaller baffle angles, particularly at Mach numbers 0.6 and 0.8 (Fig. 10b). The wire mesh overlay attenuated the noise and yielded a sound pressure level similar to that of the other configurations with the wire mesh overlay.

4.1.5 Effects of Screen Overlay and Baffle Angles

The differences in spectra for the standard depth baffles with and without screen are shown in Fig. 11. The screen was effective in suppressing both the high-frequency, wall-generated noise and the low-frequency, wall/plenum-coupled resonance. At all test conditions the noise spectra with the screen overlay was regular and devoid of any significant discrete frequency spikes.

In summary, a comparison of the noise levels measured with each configuration is given in Fig. 12 as a function of baffle angle at discrete Mach numbers. Without the screen, $\Delta C_{p_{rms}}$ increases with increasing baffle angle. With the screen, the noise level is comparable to that obtained with solid walls.

4.2 FLOW GENERATION

The longitudinal distributions of pressure coefficient at the sidewall centerline are given in Fig. 13 for the 0-deg baffle without screen and the 45-deg baffle with screen. At subsonic Mach numbers, wall divergence would alleviate the longitudinal gradient as evidenced by the results shown in Fig. 14. However, most data were obtained with parallel top and bottom walls. The effects of wall configuration on the pressure distribution at $M_c = 1.2$ are presented in Fig. 15. Increased baffle angle resulted in decreased flow uniformity to such an extent that the 60-deg baffle was deleted from the remaining test plan. The degradation in flow uniformity (at constant wall angle) with increasing baffle inclination is distinctly illustrated in Fig. 16 using the figure of merit, ΔM_{CL} . Use of the screen overlay generally improved the longitudinal flow uniformity whereas increased baffle depth had little effect.

The difference between the average centerline Mach number and the equivalent plenum Mach number would normally be used as the tunnel calibration parameter. The effect of wall configuration on this parameter is presented in Fig. 17. One of the desired attributes of any wall modification is that the change in tunnel operating parameters be minimal. Baffle angle changes significantly change the tunnel calibration parameter whereas application of the screen overlay tends to eliminate the effect of baffle angle.

4.3 WAVE CANCELLATION

The pressure distributions on the wedge-plate bottom wall are illustrated in Fig. 18 for the 0-deg baffle without screen and the 45-deg baffle with screen overlay. If the ventilated wall is capable of wave cancellation, then the distribution would be smooth downstream of the shoulder of the wedge (station 13), and for Mach numbers of about 1.1 and above the ideal distribution would be a constant value. For these two wall configurations, reasonably good wave cancellation is evident up to a Mach number of 1.2.

The effect of wall configuration on the wedge-plate pressure distributions at $M_\infty = 1.2$ is presented in Fig. 19. The relative wave cancellation properties of the individual walls can be clearly illustrated by the figure of merit, ΔM_w , as shown in Fig. 20. The generally optimum baffle angle for wave cancellation is zero, although some slight improvement could be obtained if baffle angle could be varied as a function of Mach number, including downstream inclination. The screen overlay tends to improve the wave cancellation properties whereas baffle depth does not appear to be a significant variable.

4.4 WALL CHARACTERISTICS

As discussed in Section 3.3, the characteristics of the ventilated walls were defined by measuring the static pressure distribution at the boundary of a two-dimensional flow and then computing the compatible distribution of flow angle and the desired, or "interference-free," distributions of both the pressure coefficient and flow angle in the vicinity of the ventilated wall. Representative results are given in Fig. 21 for the 0-deg baffle and the 45-deg baffle, the latter with and without screen overlay. The effect of the screen overlay on the wall characteristics is shown more vividly in terms of the C_p - θ locus as given in Fig. 22. With the screen, the characteristics are basically linear, whereas without the screen the characteristics approach the condition required for interference-free flow. This effect is quantified in Fig. 23 using the figure of merit, $\Delta(C_p, \theta)$. Use of variable baffle angle at subsonic Mach numbers would apparently yield almost a twofold reduction in wall interference relative to the 0-deg baffle or to any baffle angle with screen overlay.

5.0 CONCLUDING REMARKS

An experimental investigation was conducted to document the acoustic and aerodynamic properties of baffle-slot wall configurations with and without screen overlays.

The test section sound pressure level was a minimum for the 0-deg (normal) baffle and generally increased with increasing baffle angle. There was a discrete frequency, resonant spike for the 15-deg baffle configuration near Mach number 0.5 which caused a significantly high sound pressure level. The frequency content of the wall-induced acoustic disturbances which contributed to the test section overall noise level was predominantly low frequency for baffle angles of 30 and 45 deg, broadband for zero baffle angle, and generally broadband for 15-deg baffle angle with some discrete high frequency tones. The wire mesh screen overlay was effective for suppressing the wall-induced disturbances for all the baffle configurations and yielded essentially the same sound pressure level as the solid wall configuration.

In summary, increasing baffle angle 1) adversely affected flow generation and wave cancellation properties of the wall, yet 2) improved subsonic interference properties and 3) effected significant changes in the wall characteristic. In each case, however, application of the screen overlay eliminated baffle angle as a significant variable.

REFERENCES

1. Dougherty, N. S., Jr. and Steinle, F. W., Jr. "Transition Reynolds Number Comparisons in Several Major Transonic Tunnels." AIAA Paper No. 74-627, July 1974.
2. Dougherty, N. S., Jr. "A Study of Acoustic Disturbances and Means of Suppression in Ventilated Transonic Wind Tunnel Walls." AEDC-TR-77-67 (ADA045347), October 1977.
3. Dougherty, N. S., Jr., Anderson, C. F., and Parker, R. L., Jr. "An Experimental Investigation of Techniques to Suppress Edgetones from Perforated Wind Tunnel Walls." AEDC-TR-75-88 (ADA013728), August 1975.
4. Jacocks, J. L. "Aerodynamic Characteristics of Perforated Walls for Transonic Wind Tunnels." AEDC-TR-77-61 (ADA040904), June 1977.
5. Lo, C. F. and Kraft, E. M. "Convergence of the Adaptive-Wall Wind Tunnel." *AIAA Journal*, Vol. 16, No. 1, January 1978, pp. 67-72.

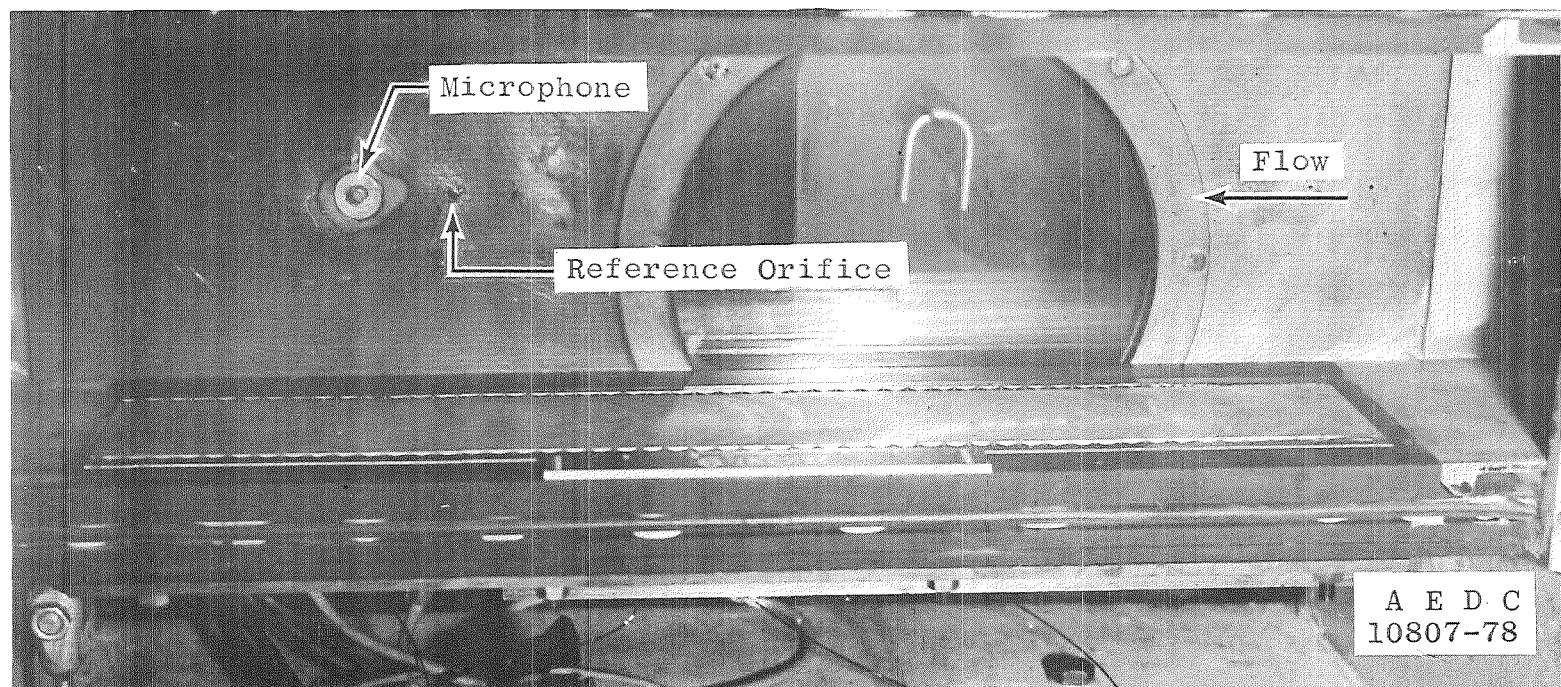
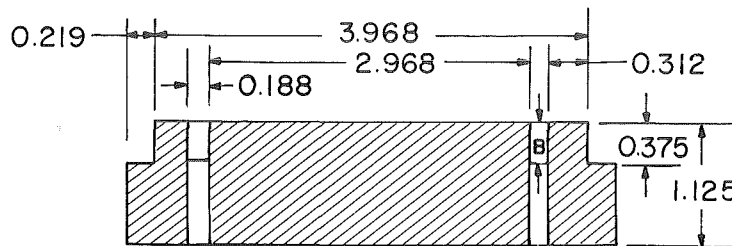
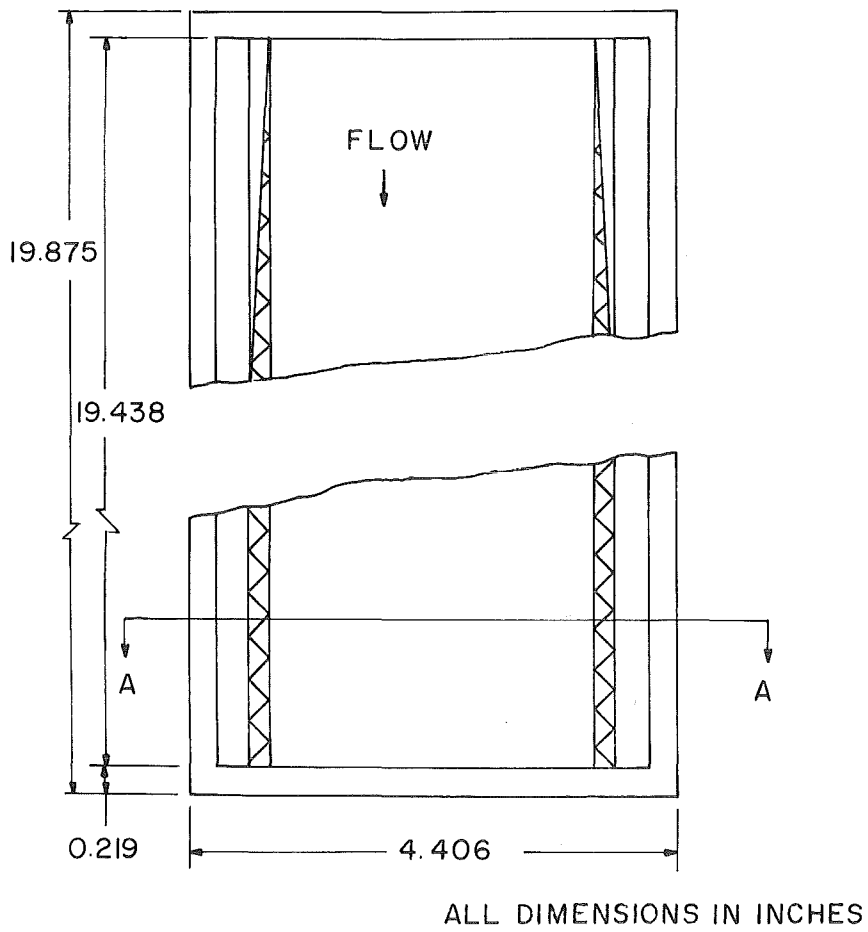


Figure 1. Acoustic research tunnel test section arrangement.



SECTION A - A

BAFFLE DEPTH	B, in.
SHALLOW	0.35
DEEP	0.70

Figure 2. Wall sample dimensions.

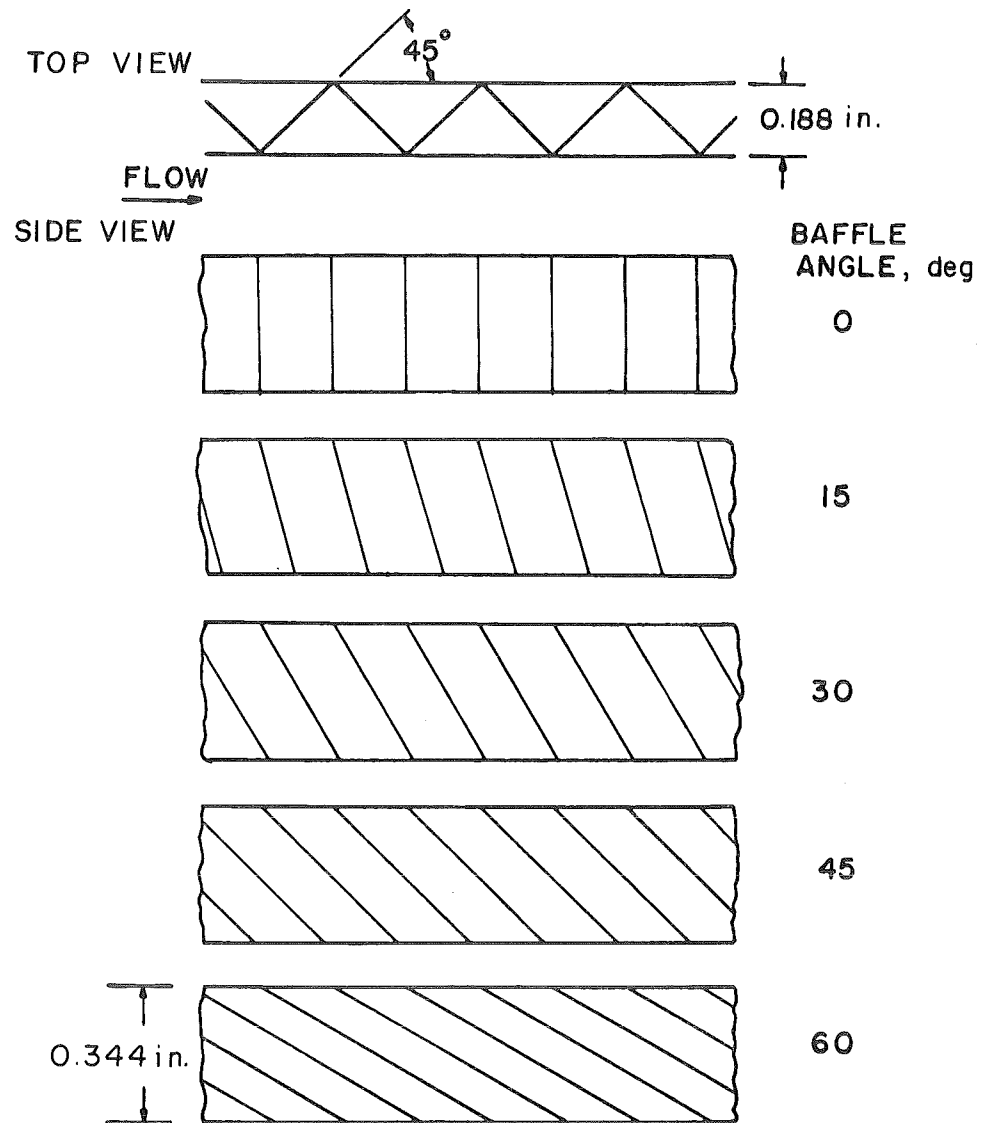


Figure 3. Baffle geometry.

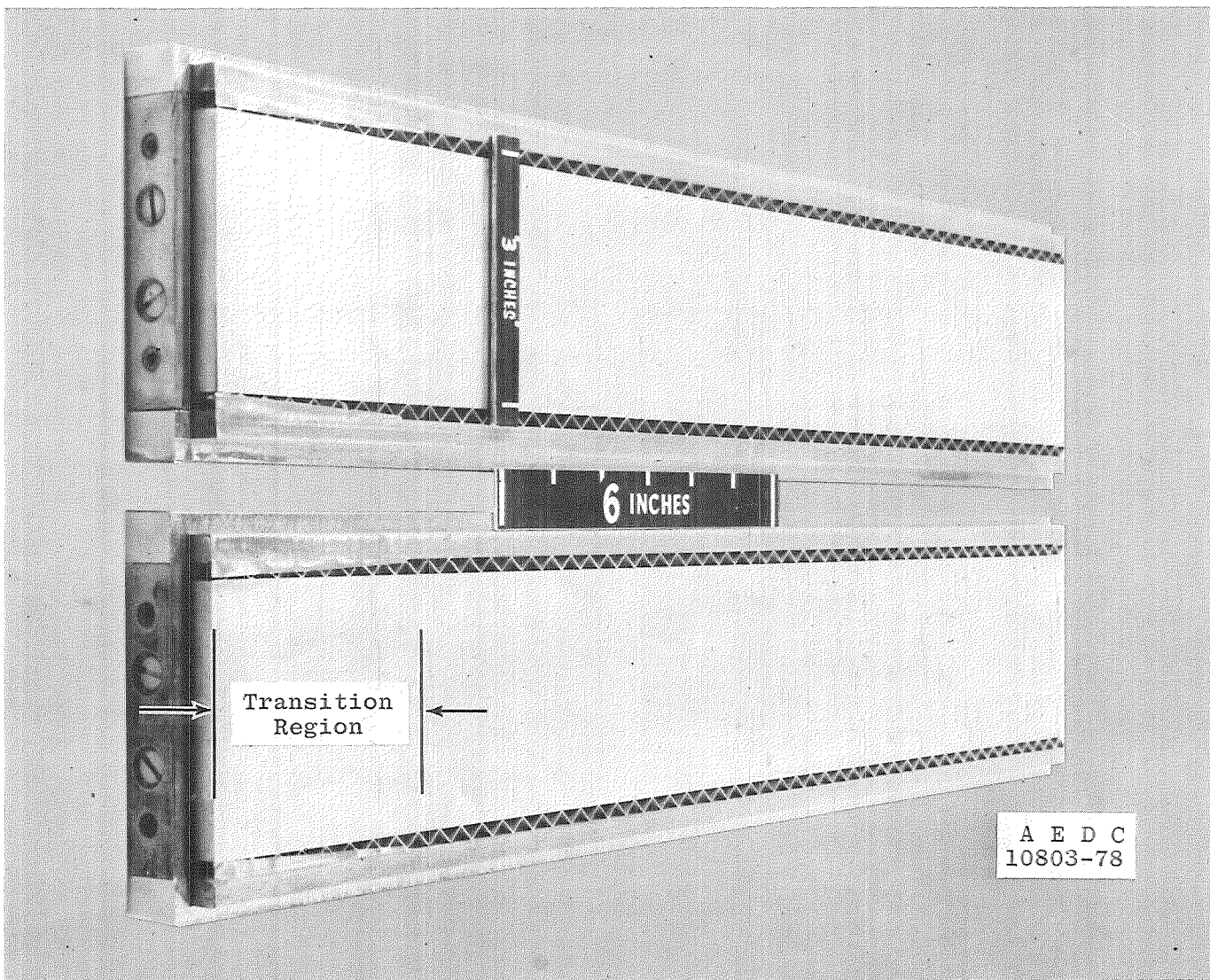


Figure 4. Top and bottom wall samples for the acoustic research tunnel.

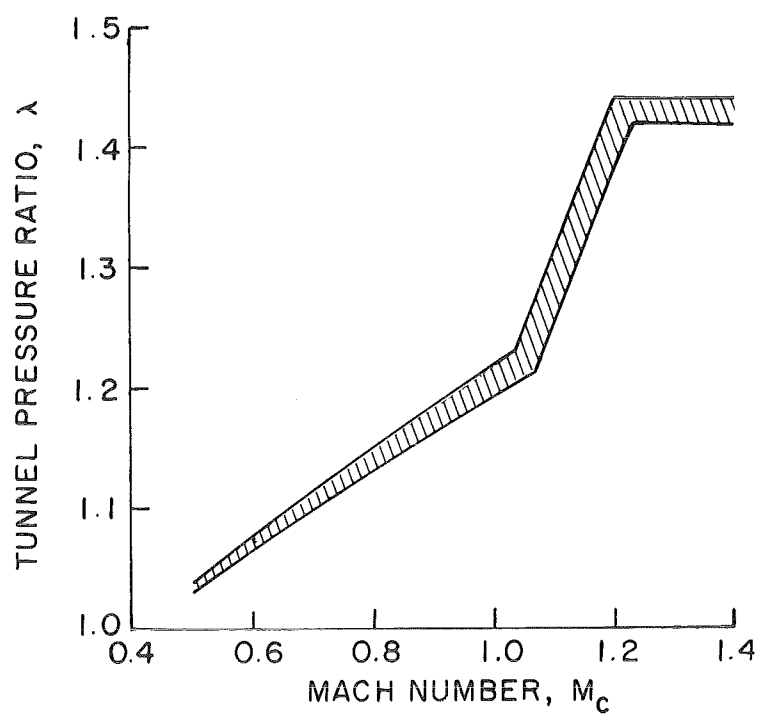


Figure 5. Tunnel pressure ratio schedule for Tunnel 1T.

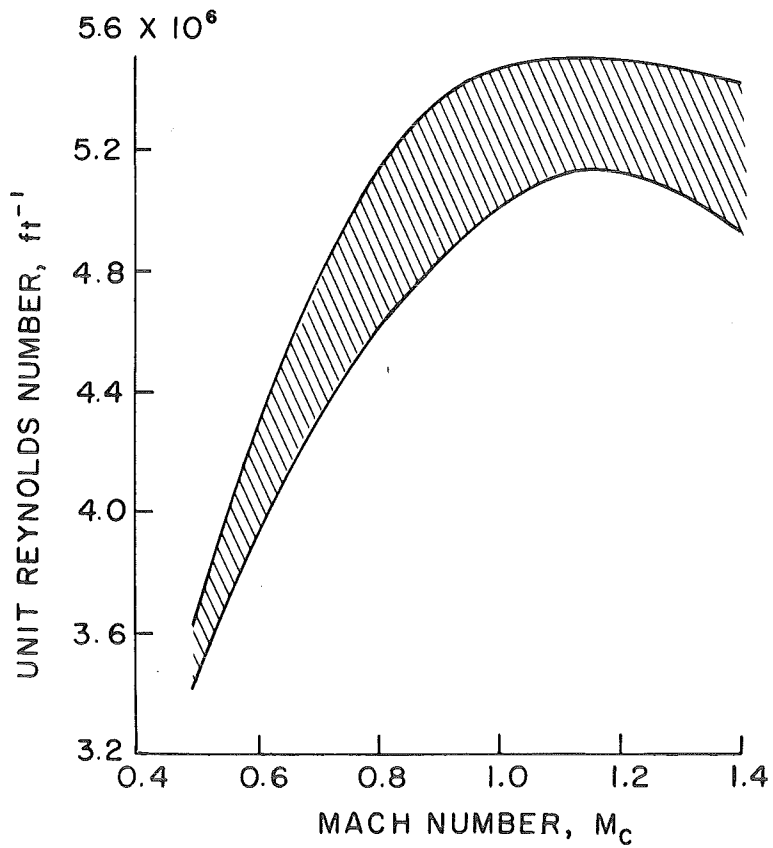
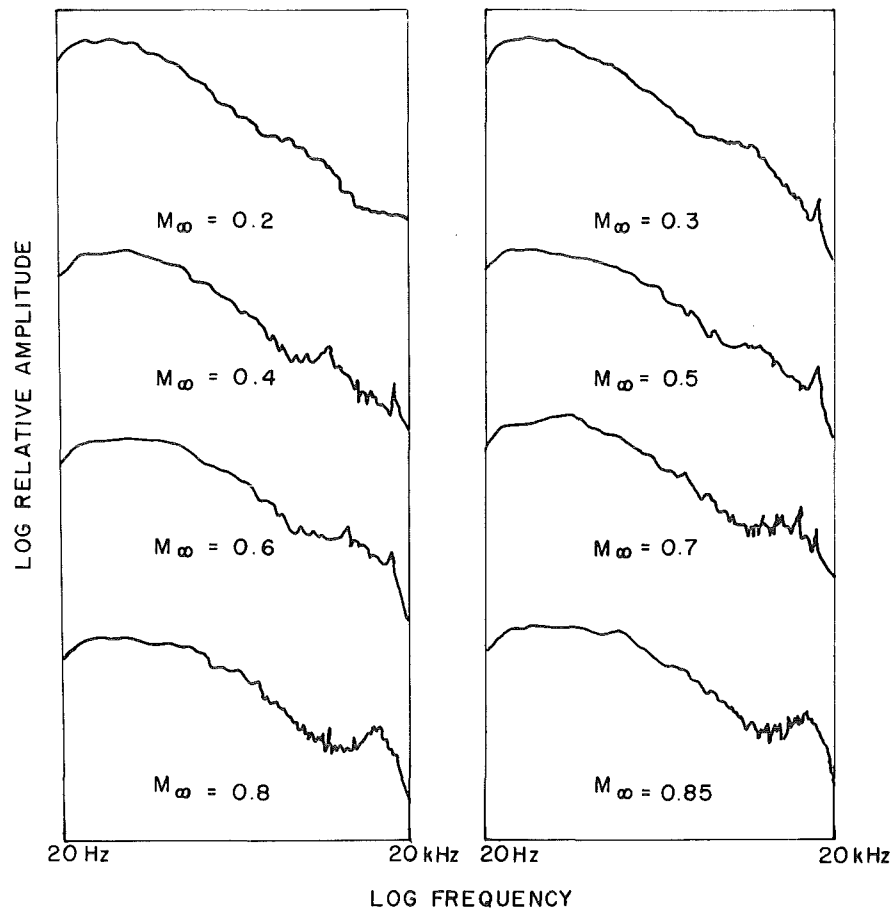
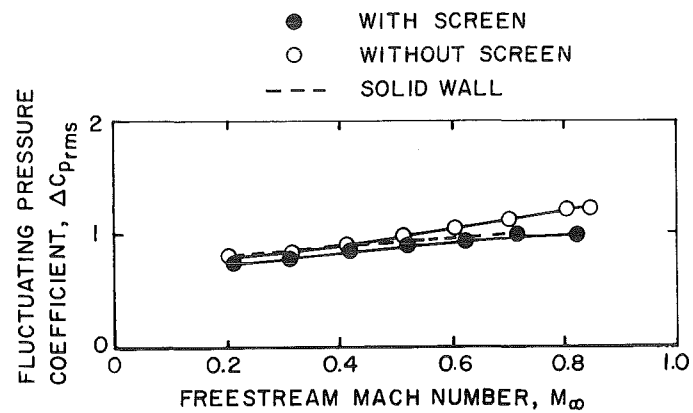


Figure 6. Reynolds number envelope for Tunnel 1T.

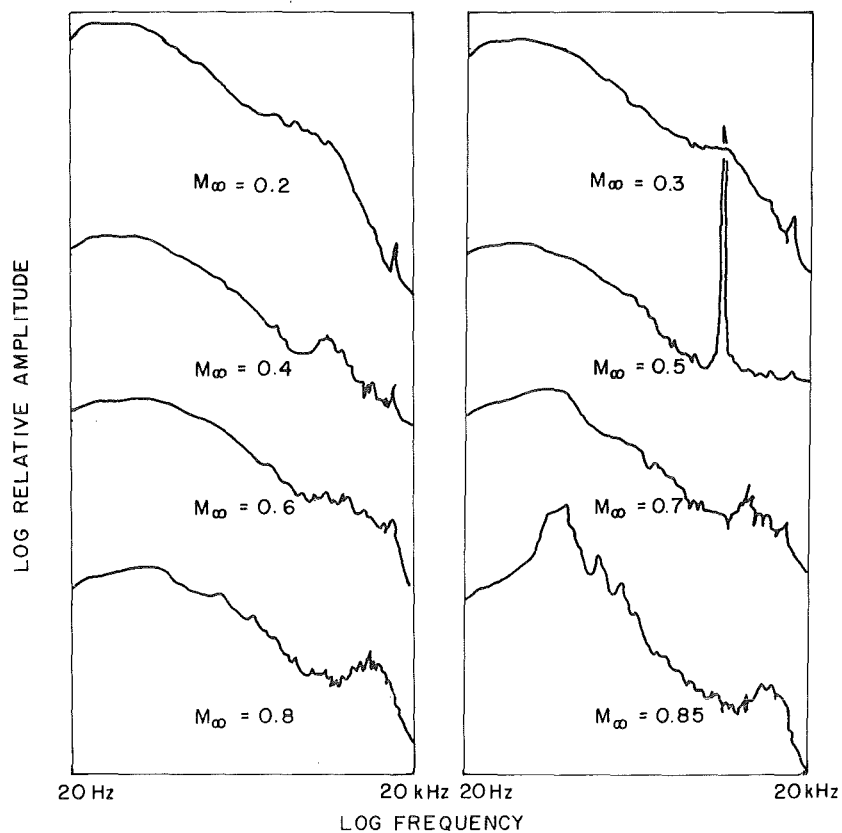


a. Spectra



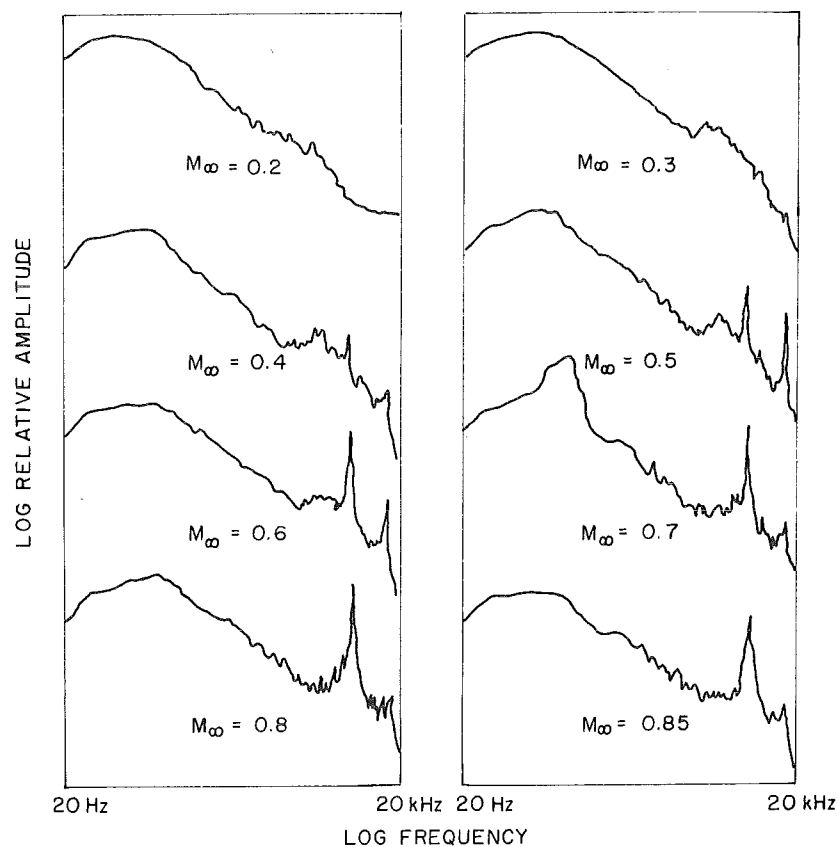
b. Overall noise level

Figure 7. Spectra and overall noise level at zero baffle angle.

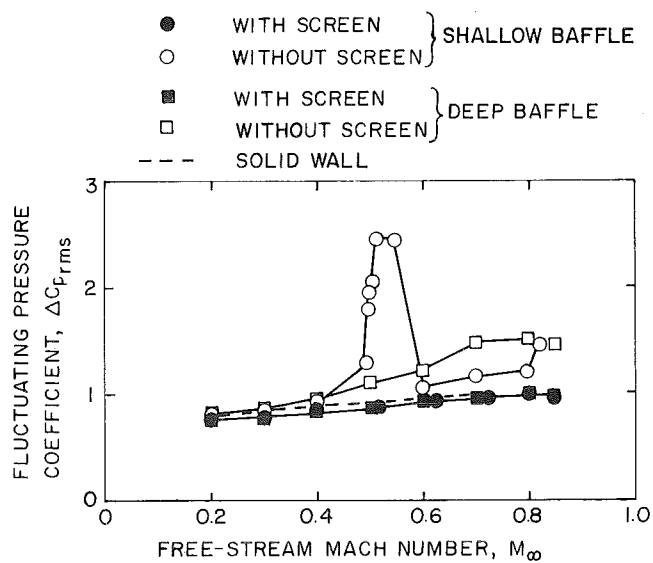


a. Spectra, shallow baffle

Figure 8. Spectra and overall noise level at 15-deg baffle angle.

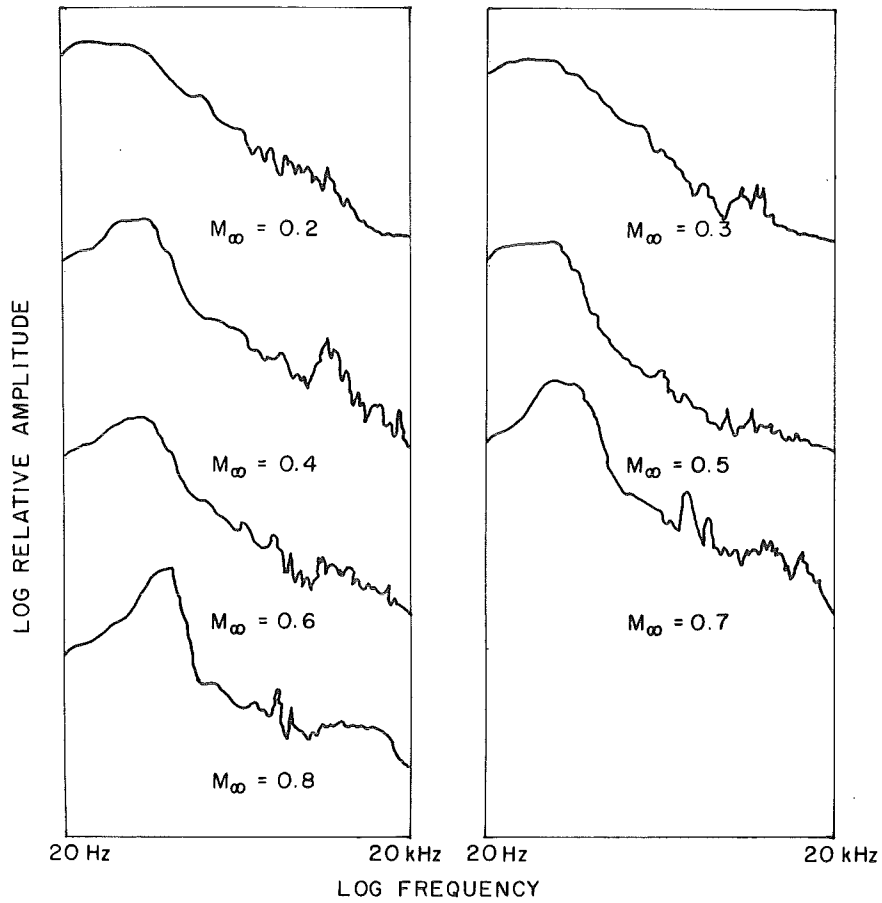


b. Spectra, deep baffle

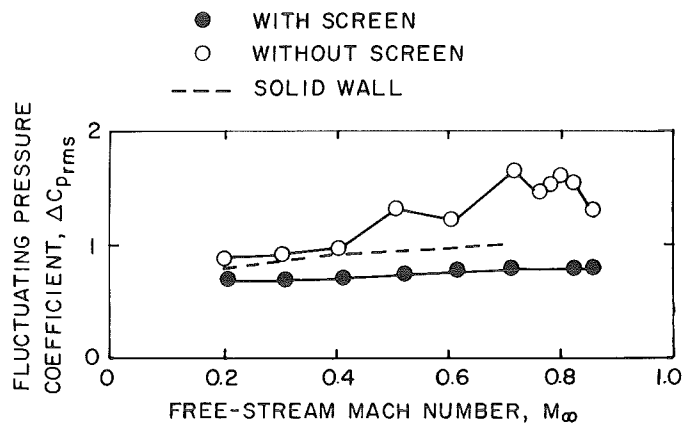


c. Overall noise level

Figure 8. Concluded.

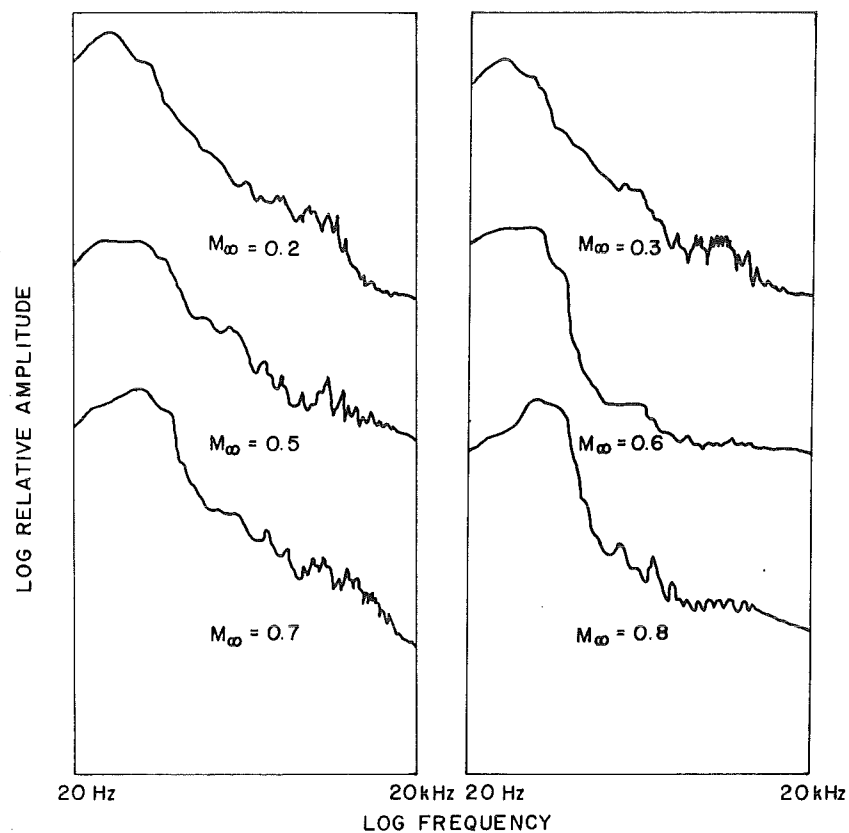


a. Spectra

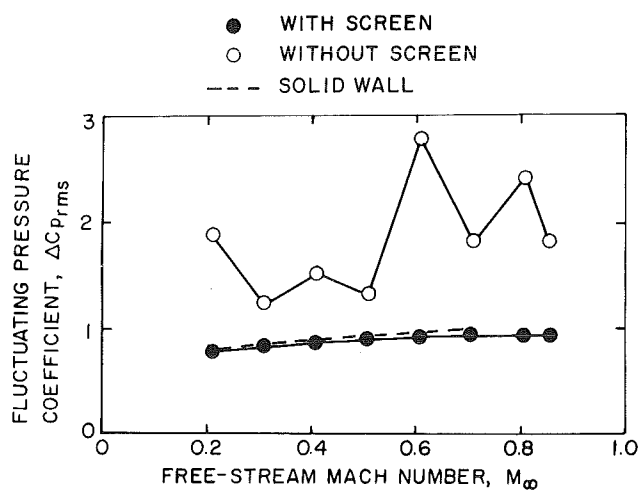


b. Overall noise level

Figure 9. Spectra and overall noise level at 30-deg baffle angle.



a. Spectra



b. Overall noise level

Figure 10. Spectra and overall noise level at 45-deg baffle angle.

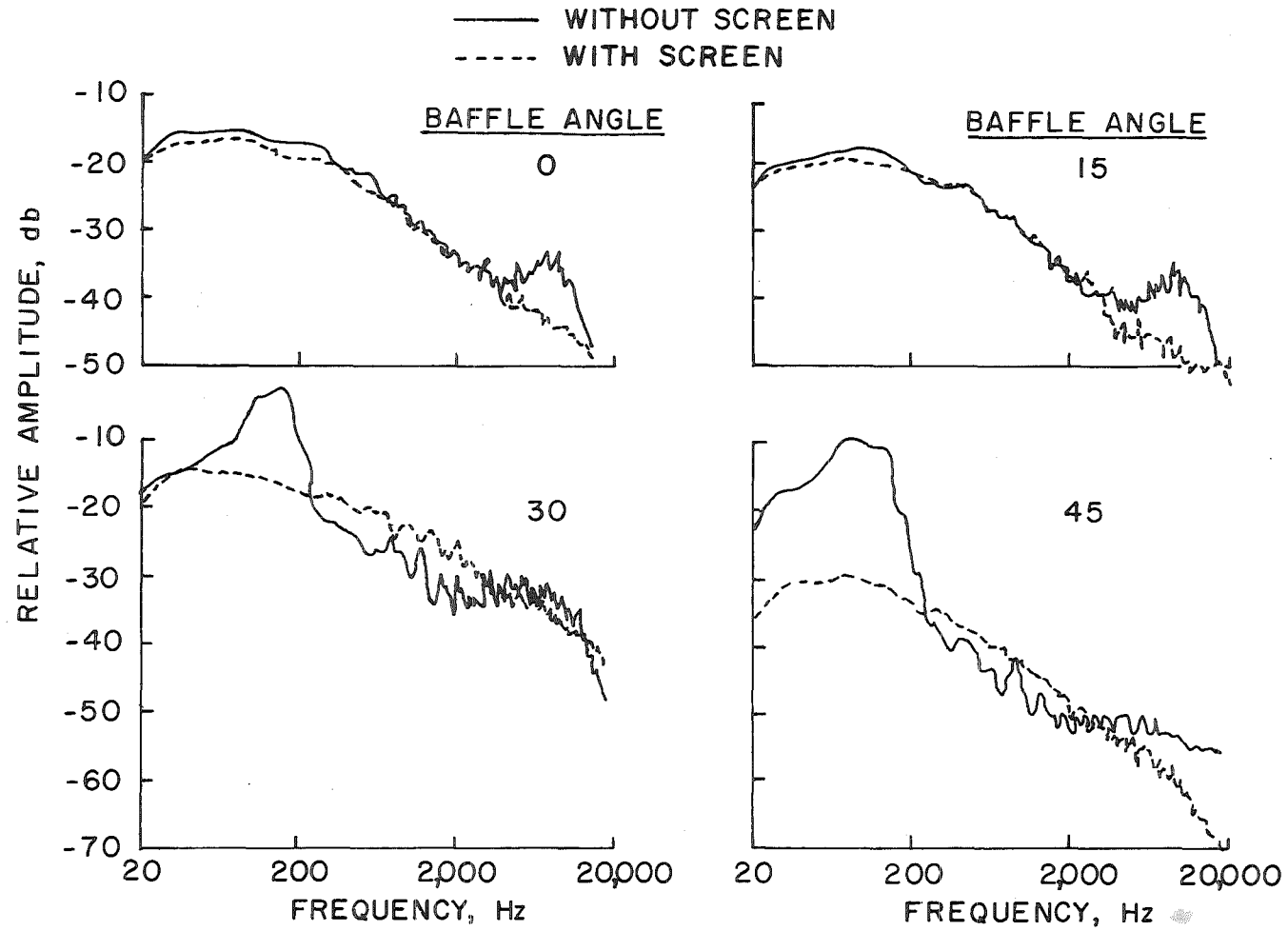


Figure 11. Effect of screen overlay on the noise spectrum.

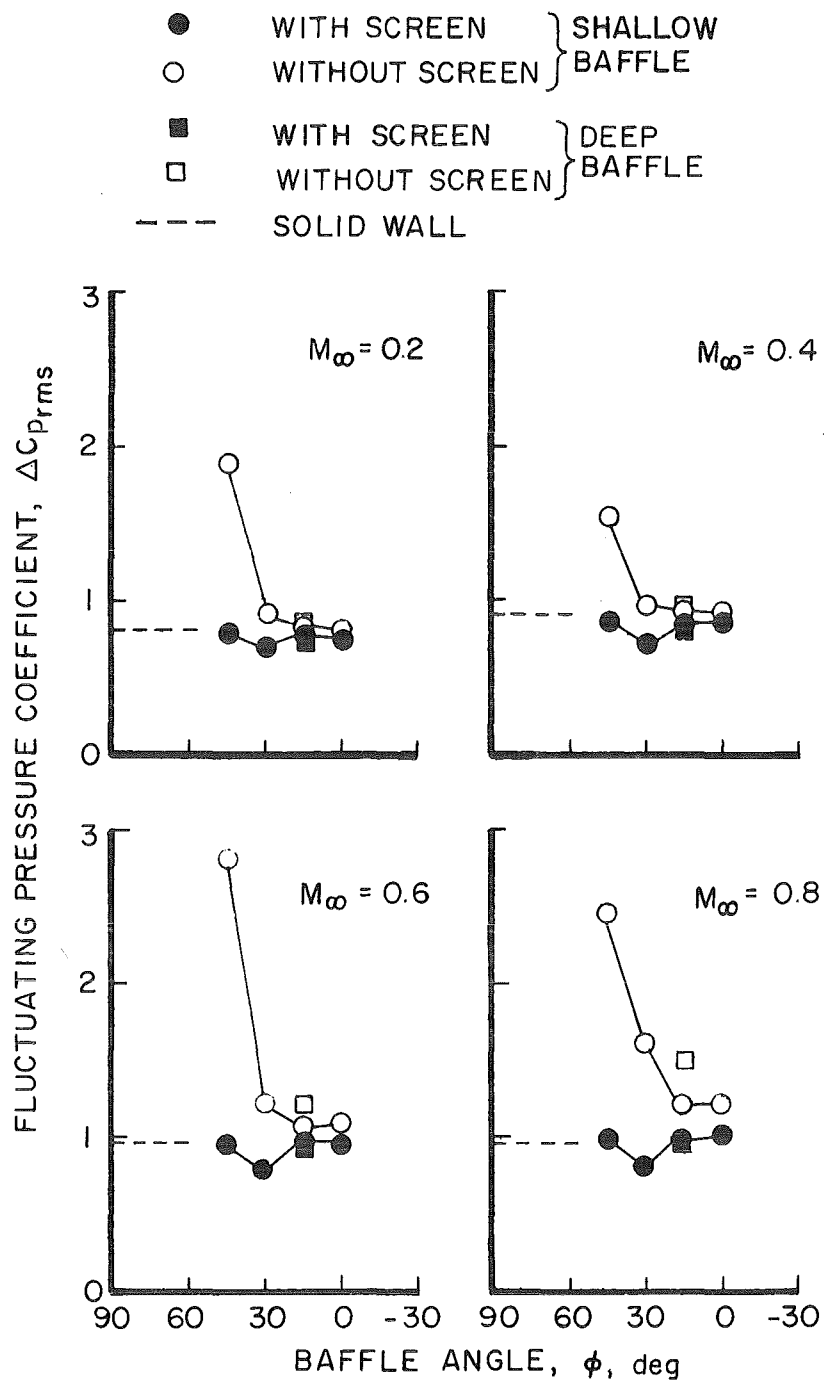
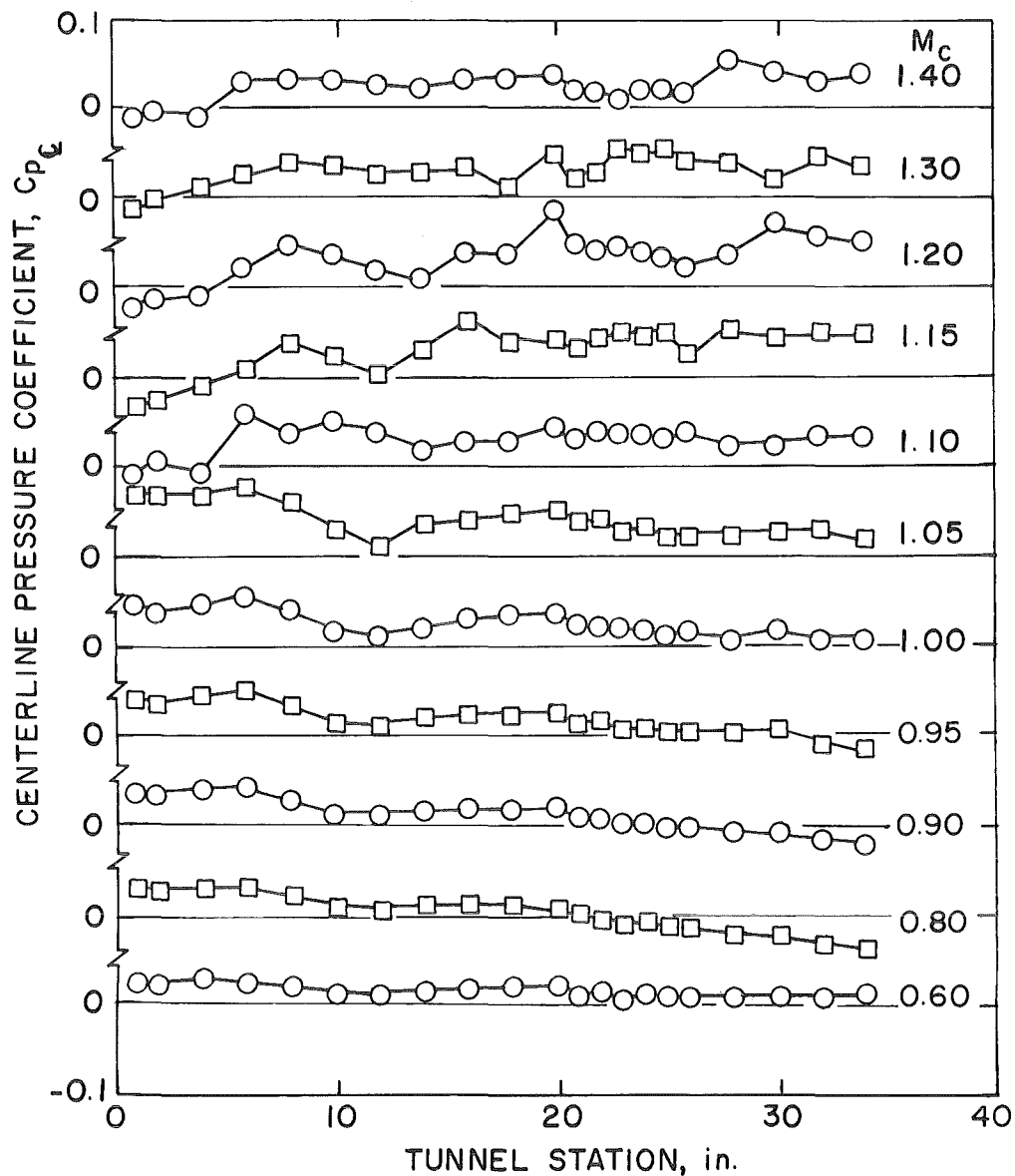
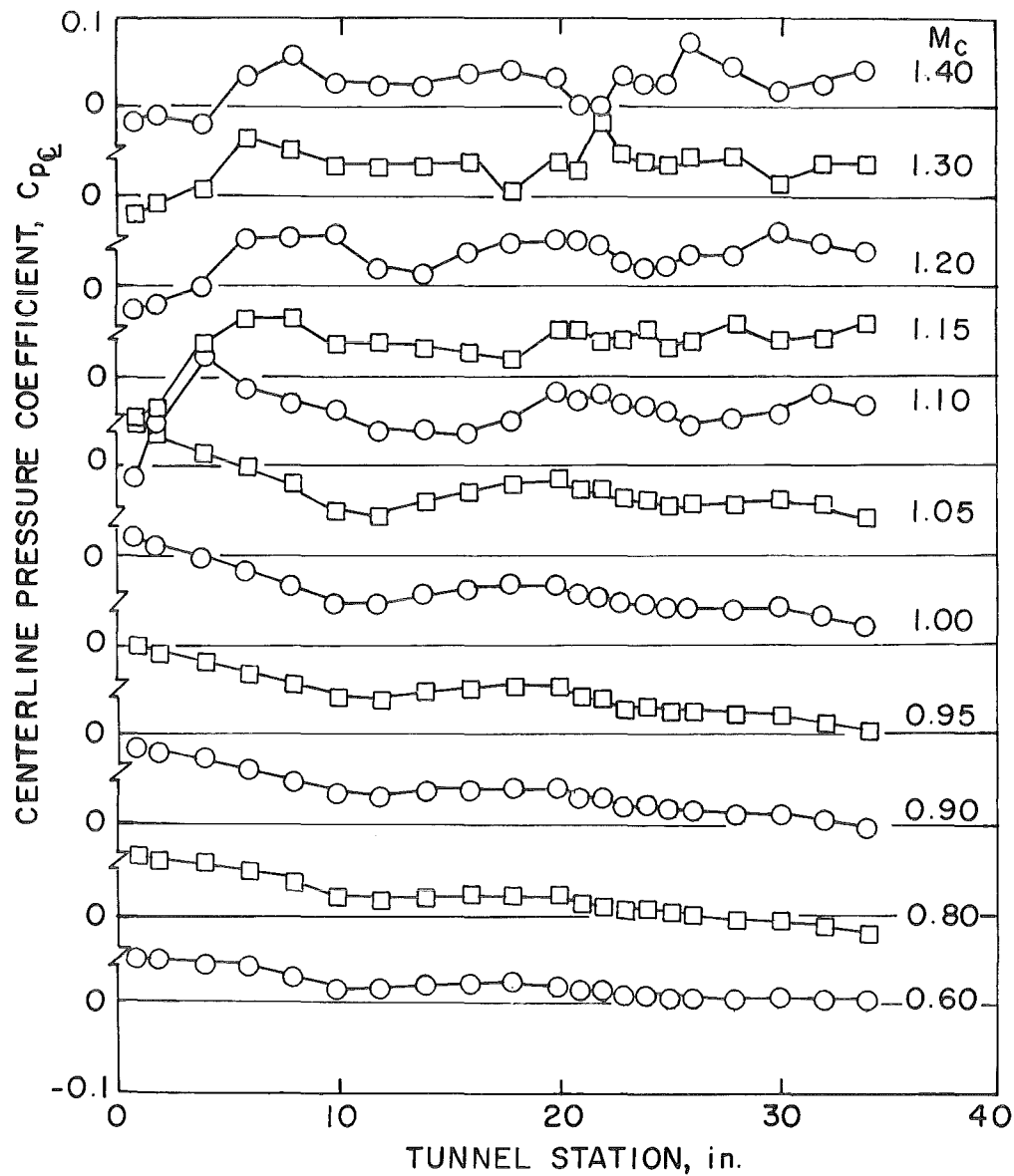


Figure 12. Effect of baffle angle on the overall noise level.



a. $\phi = 0$, without screen

Figure 13. Representative centerline static pressure distributions.



b. $\phi = 45$ deg, with screen
Figure 13. Concluded.

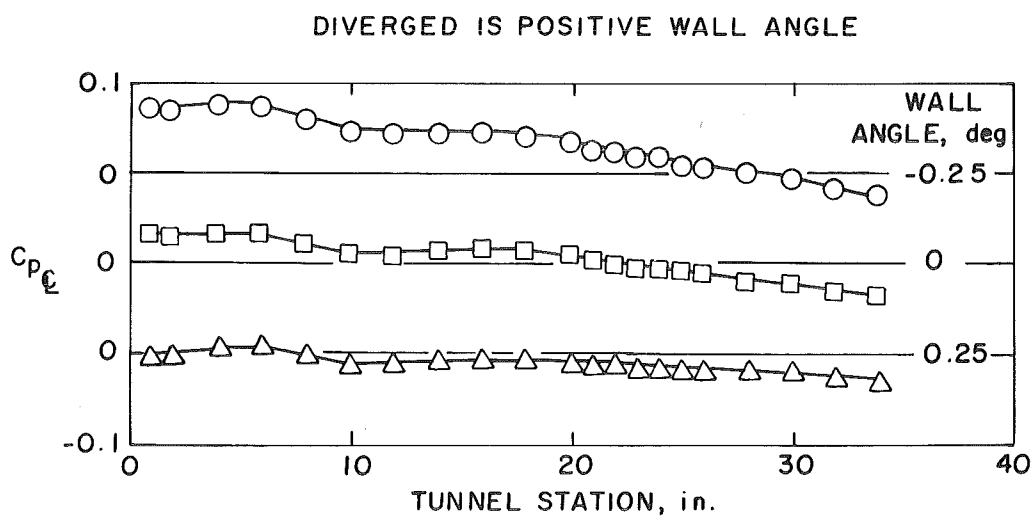


Figure 14. Effect of wall angle on the centerline static pressure distribution, $\phi = 0$, $M_c = 0.8$, screen off.

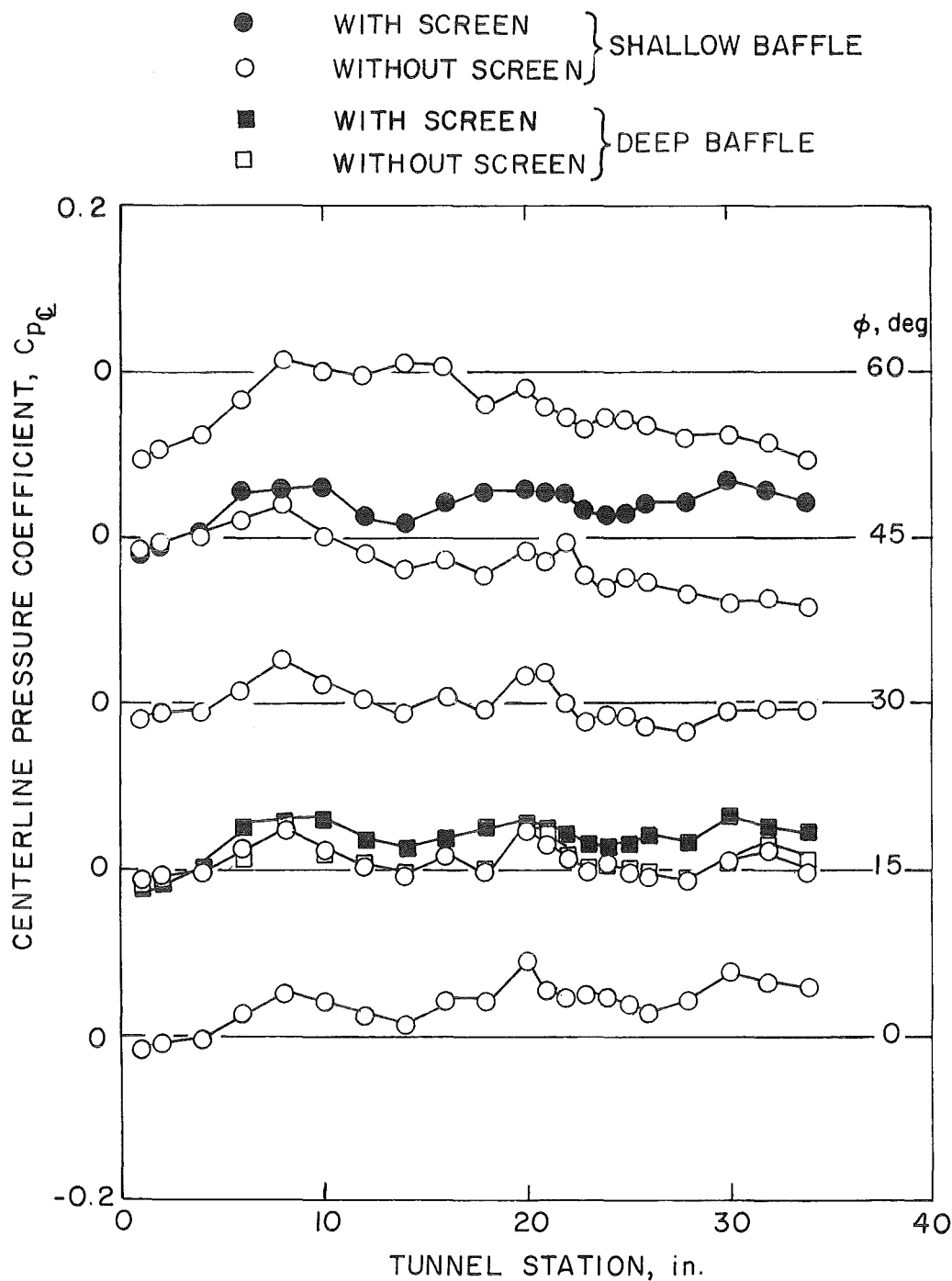


Figure 15. Effect of wall configuration on the centerline static pressure distribution, $M_c = 1.2$.

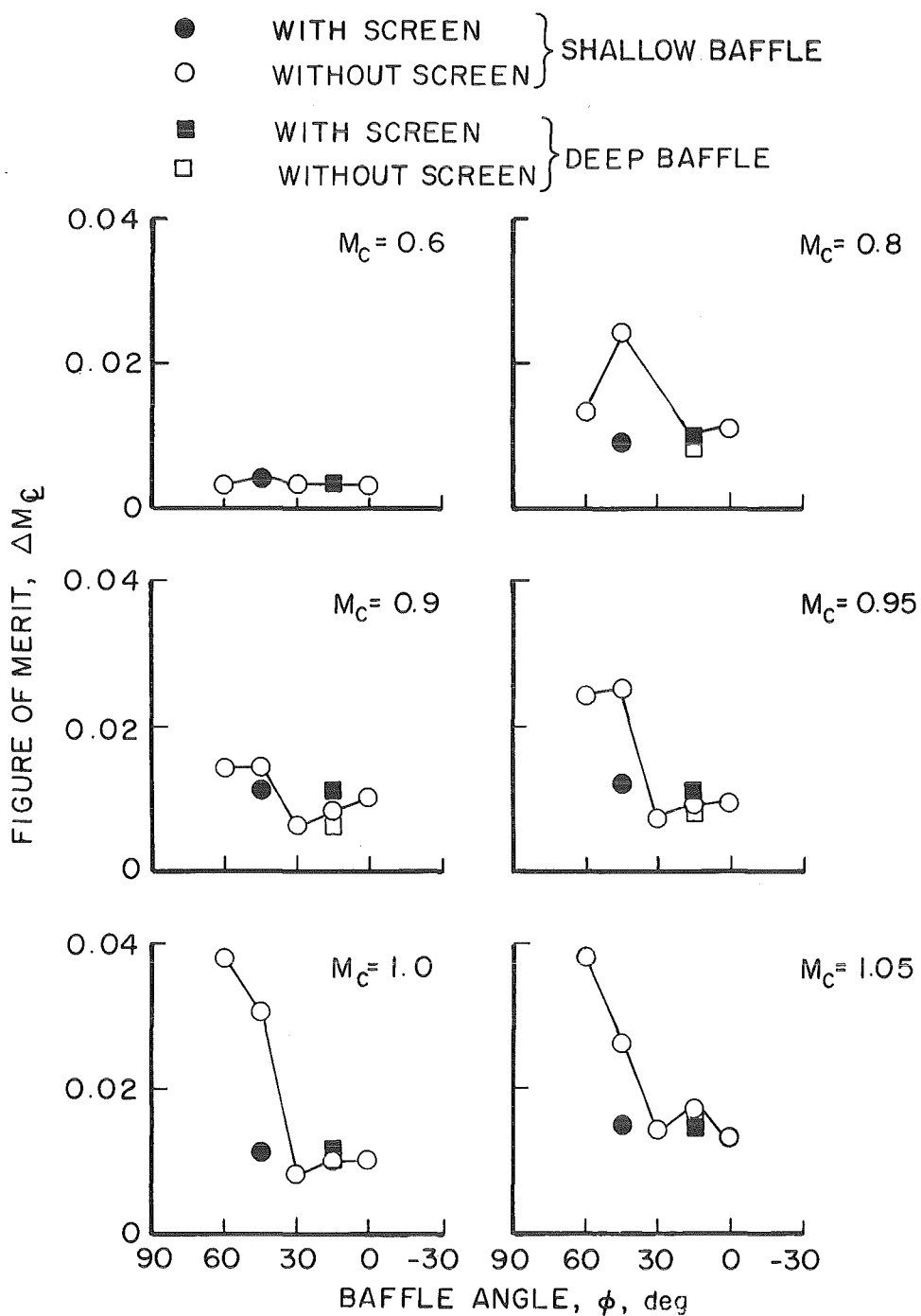


Figure 16. Effect of wall configuration on the flow uniformity figure of merit.

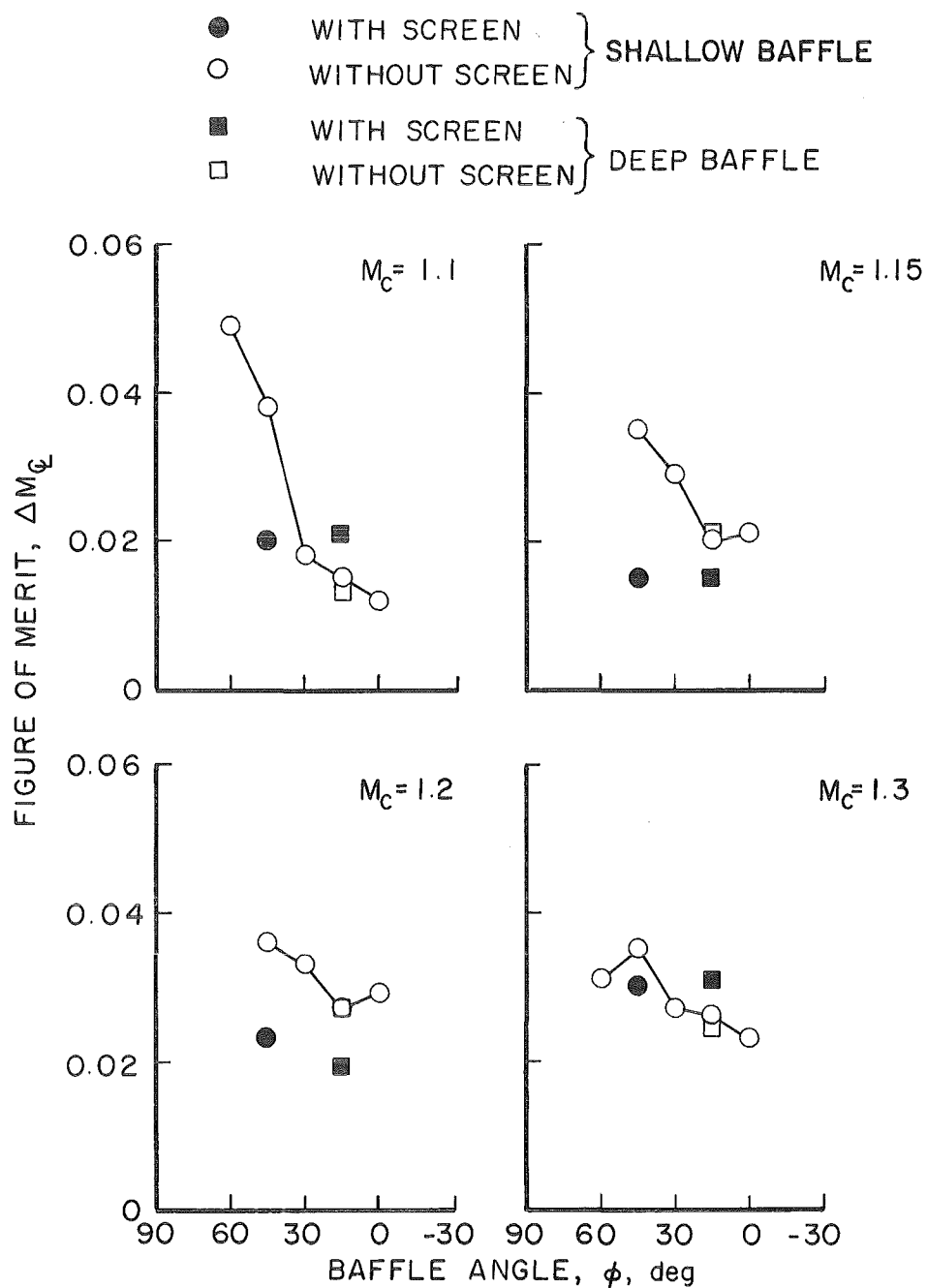


Figure 16. Concluded.

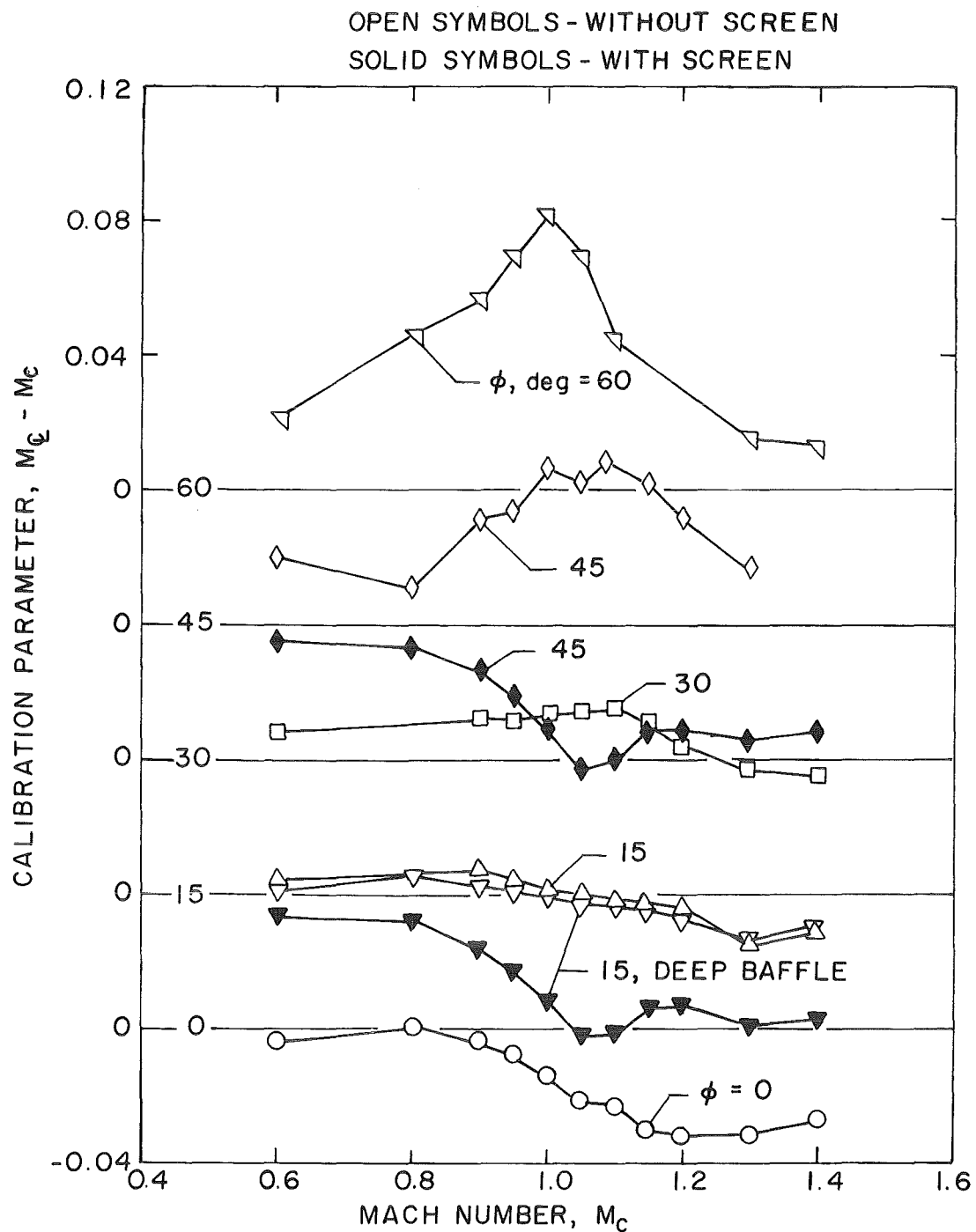
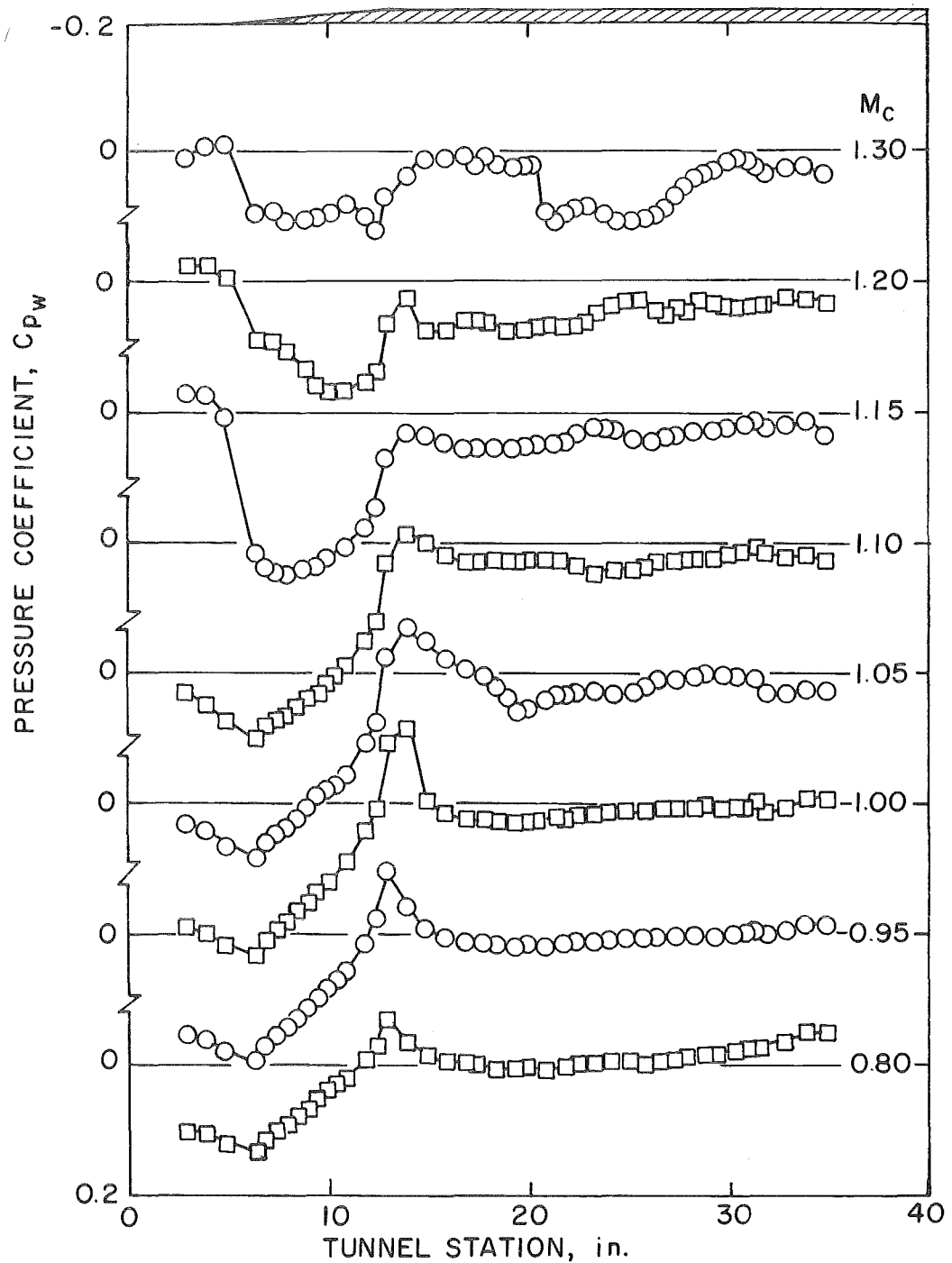
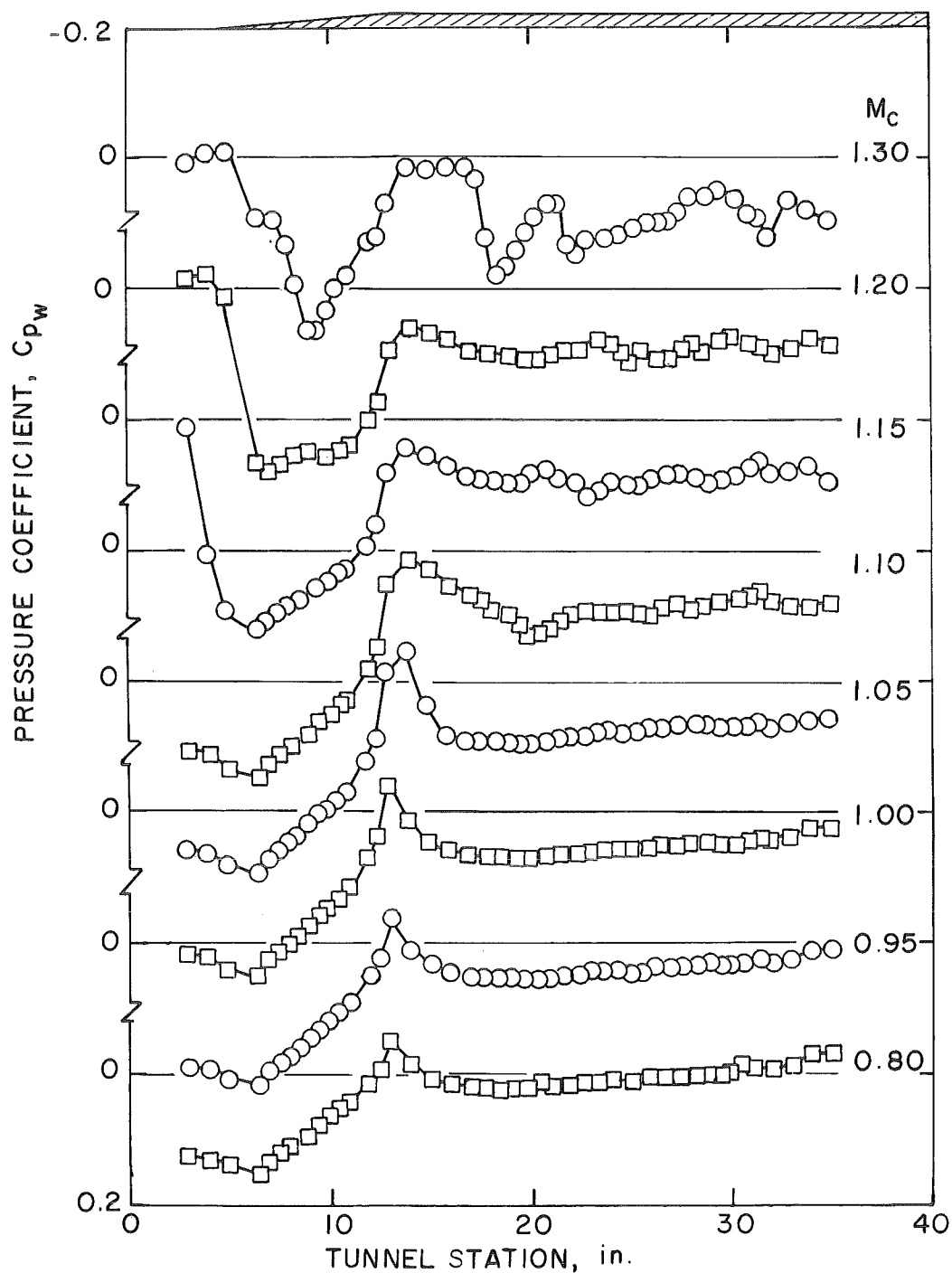


Figure 17. Effect of wall configuration on the tunnel calibration parameter.



a. $\phi = 0$, without screen

Figure 18. Representative wedge static pressure distributions.



b. $\phi = 45$ deg, with screen
Figure 18. Concluded.

OPEN SYMBOLS - WITHOUT SCREEN

SOLID SYMBOLS - WITH SCREEN

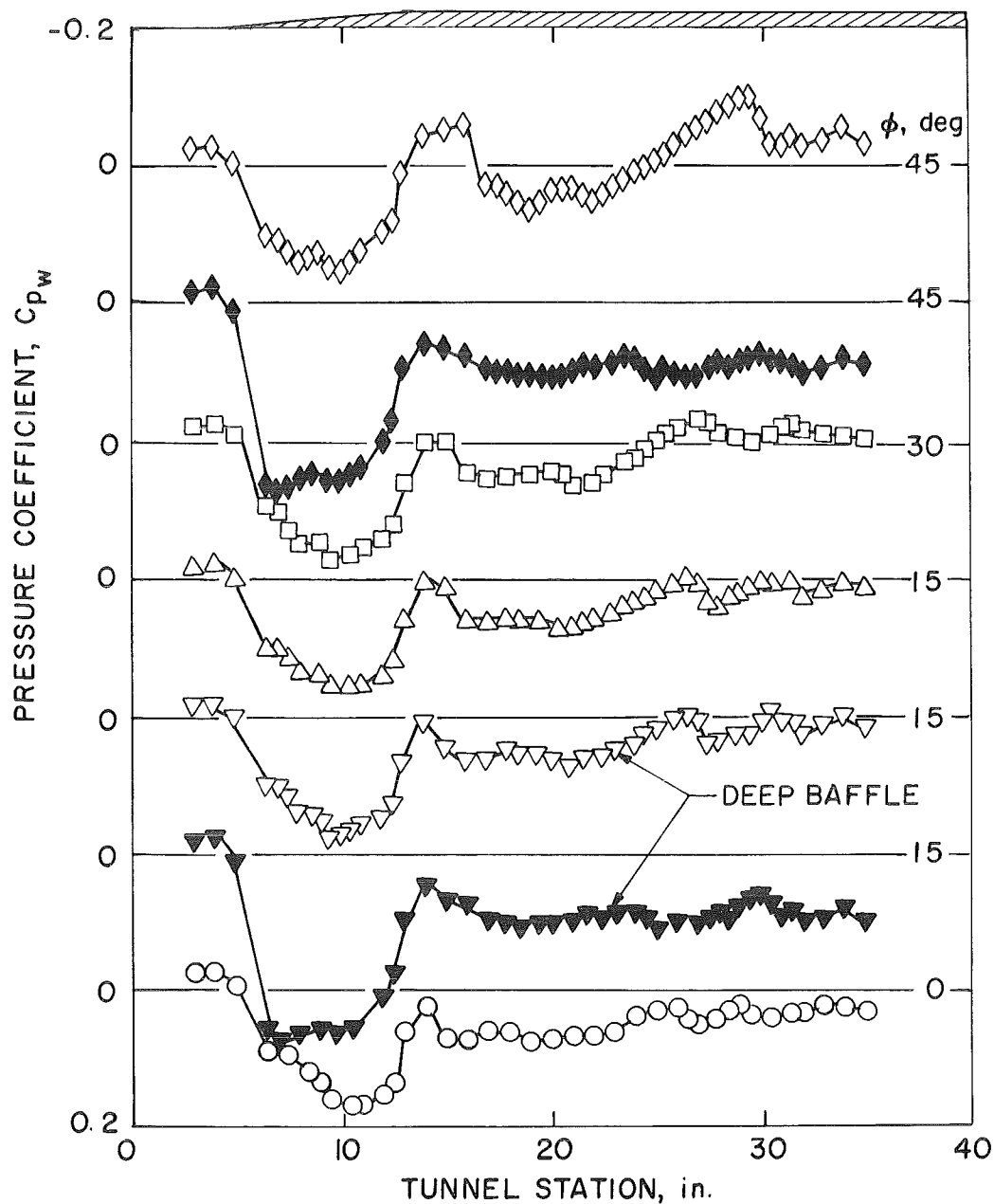


Figure 19. Effect of wall configuration on the wedge static pressure distribution, $M_c = 1.2$.

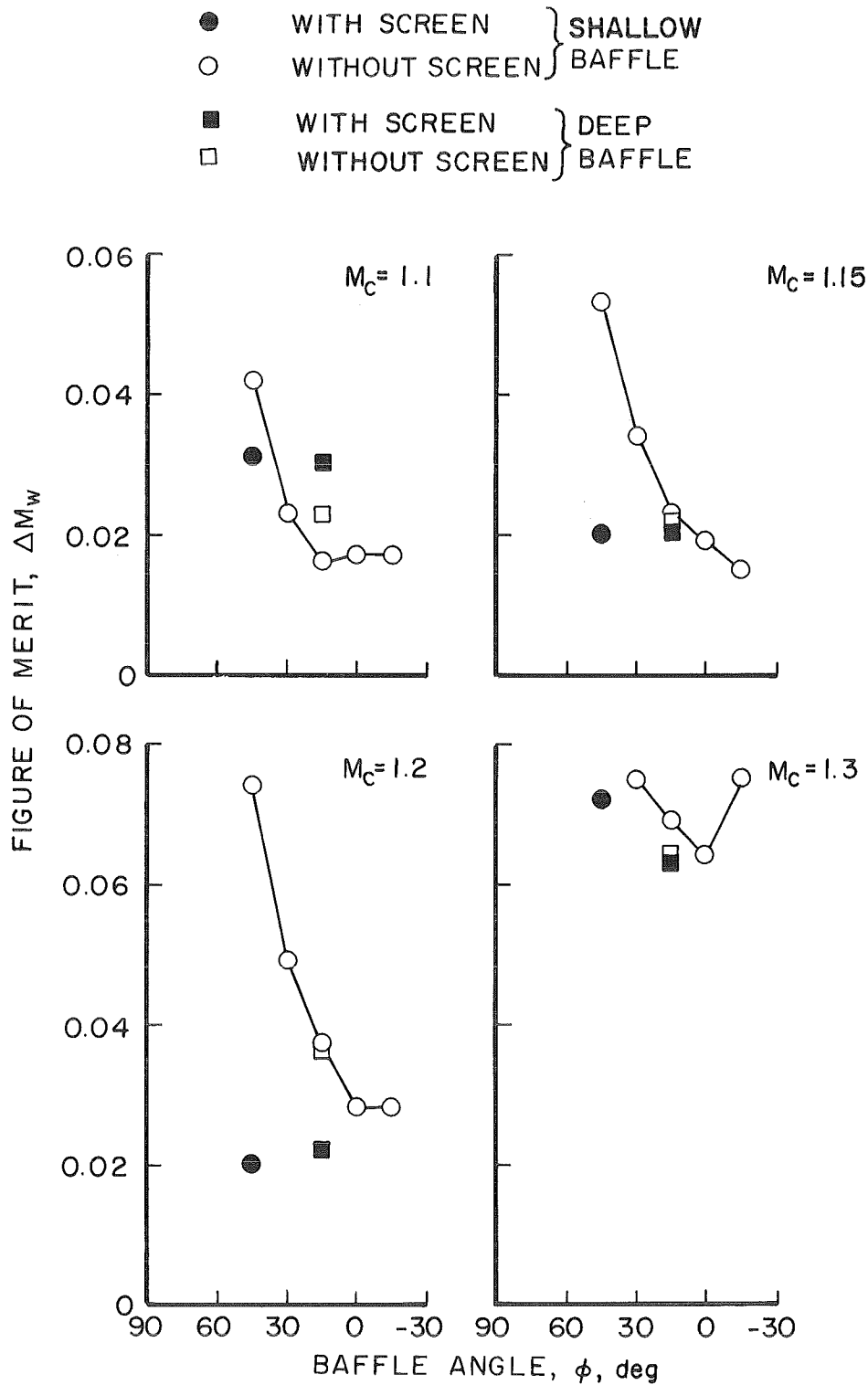
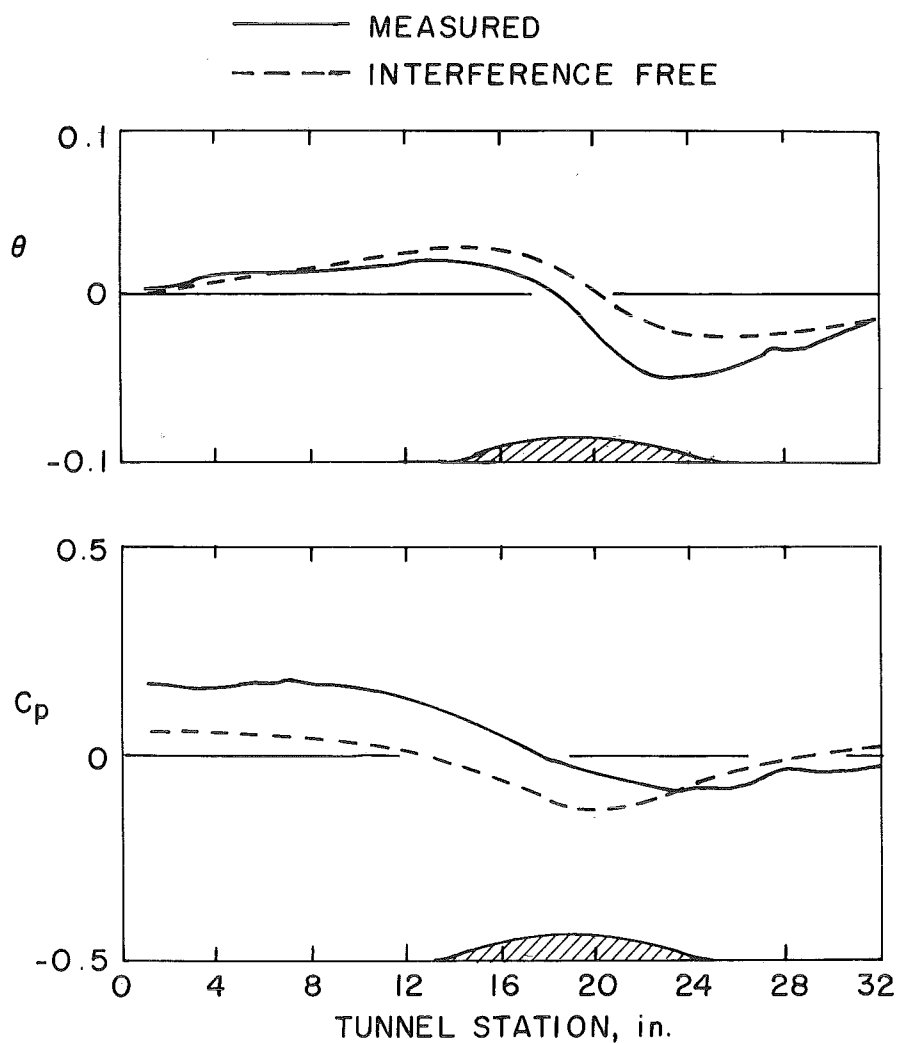
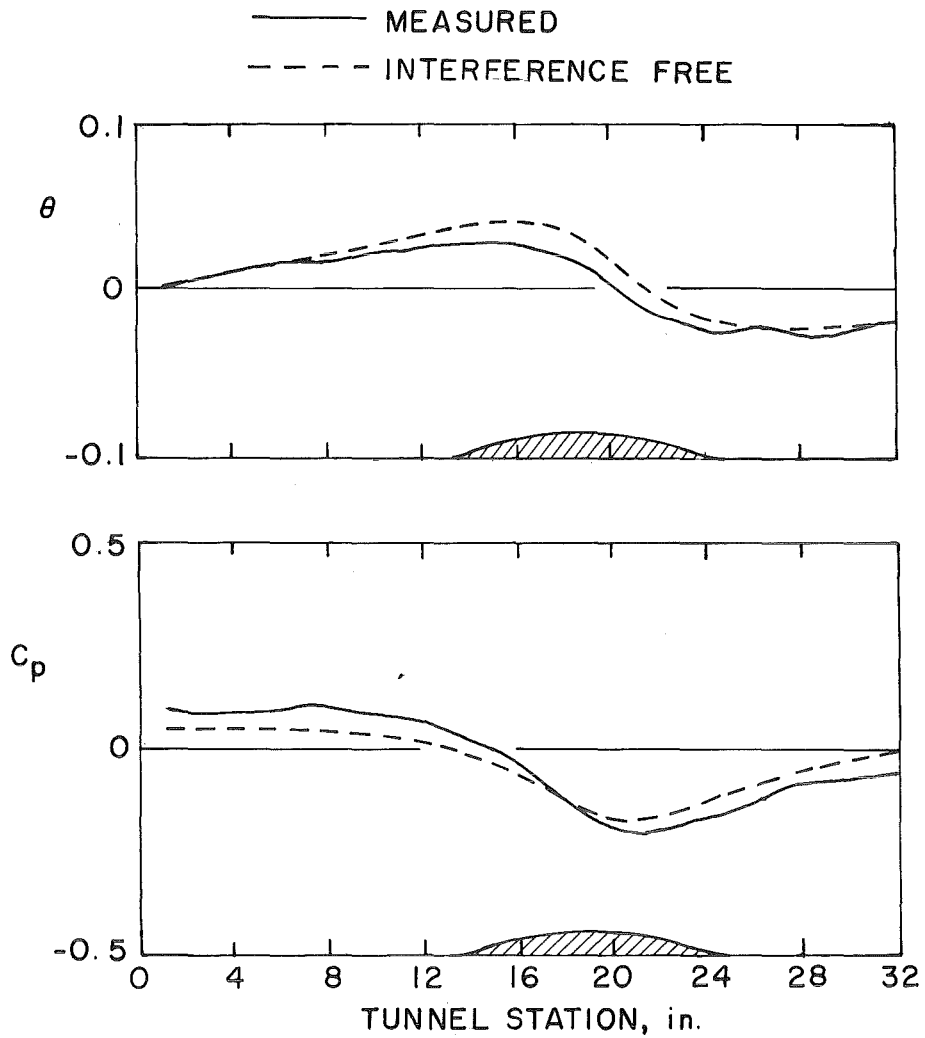


Figure 20. Effect of wall configuration on the wave cancellation figure of merit.

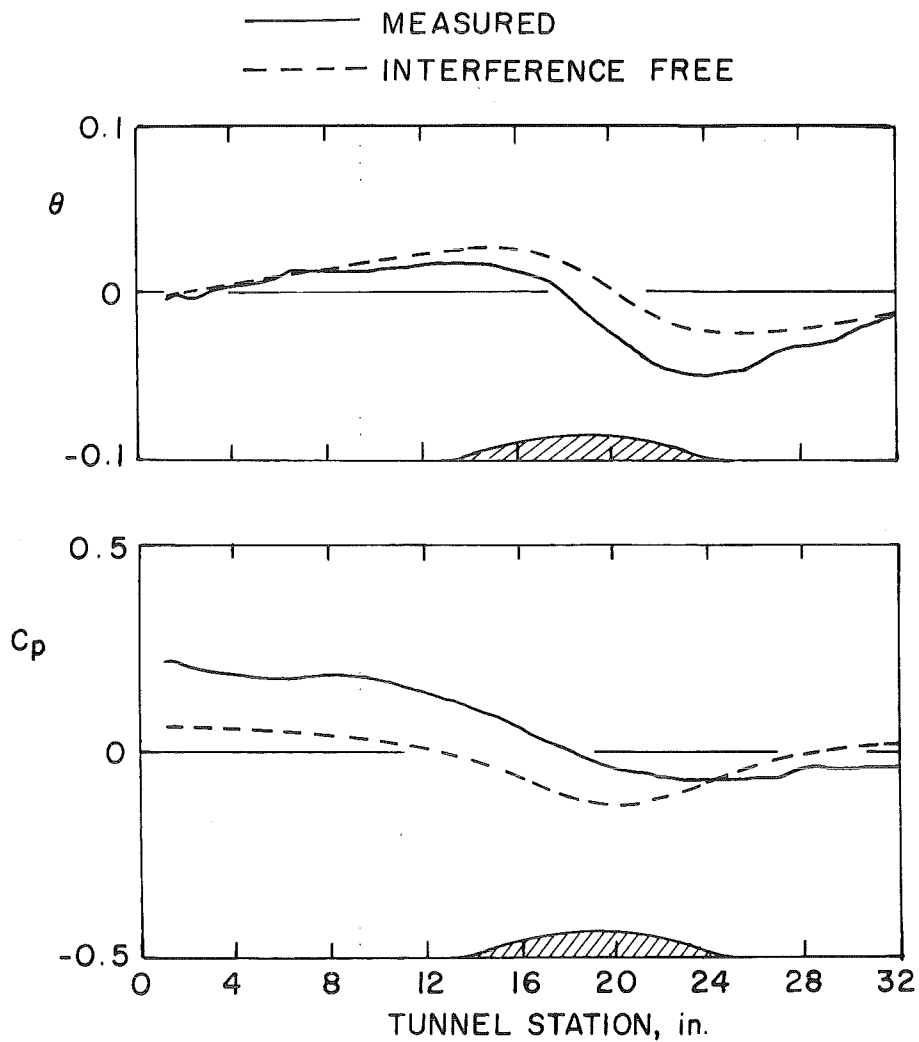


a. $\phi = 0$, without screen

Figure 21. Representative flow angle and static pressure distributions at the ventilated wall, $M_c = 0.8$.

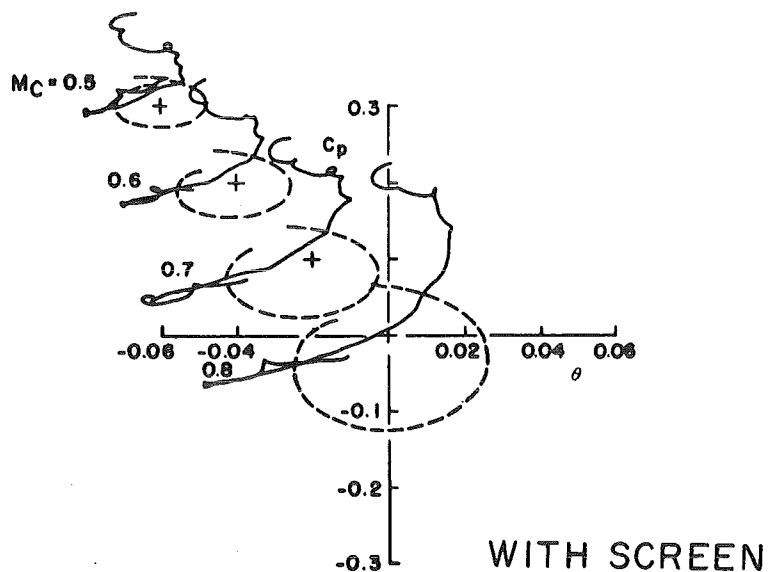


b. $\phi = 45$ deg, without screen
Figure 21. Continued.

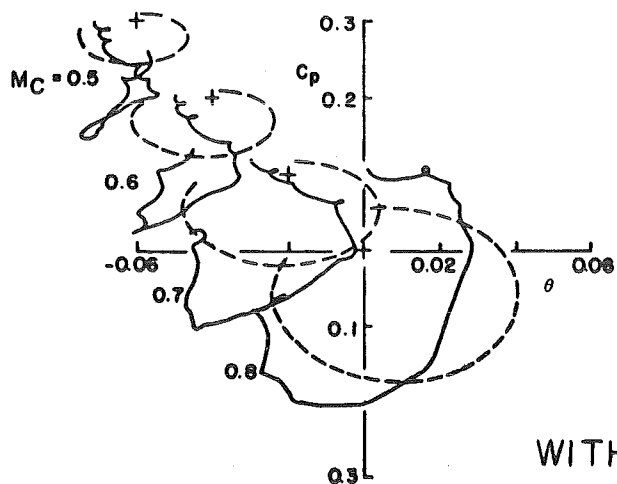


c. $\phi = 45$ deg, with screen
Figure 21. Concluded.

—— MEASURED
 ---- INTERFERENCE FREE



WITH SCREEN



WITHOUT SCREEN

Figure 22. Effect of screen overlay and Mach number on the wall characteristic, $\phi = 45$ deg.

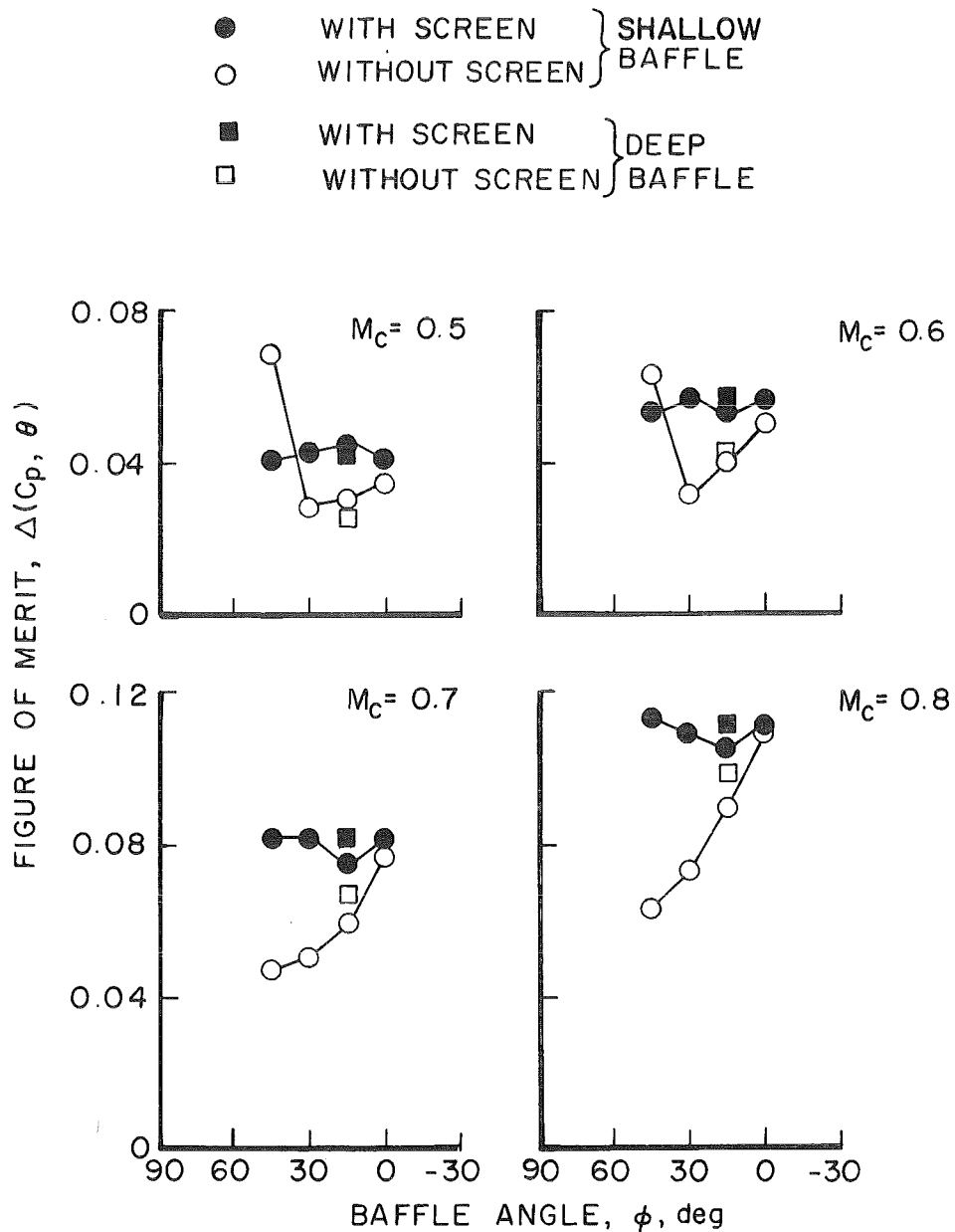


Figure 23. Effect of wall configuration on the wall interference alleviation figure of merit.

Table 1. Test Configurations

BAFFLE ANGLE, deg	BAFFLE DEPTH, in.	ACOUSTIC NOISE		FLOW GENERATION		WAVE CANCELLATION		WALL CHARACTERISTICS	
		SCREEN ON	SCREEN OFF	SCREEN ON	SCREEN OFF	SCREEN ON	SCREEN OFF	SCREEN ON	SCREEN OFF
-15	0.35						X		
0	0.35	X	X		X		X	X	X
15	0.35	X	X		X		X	X	X
30	0.35	X	X		X		X	X	X
45	0.35	X	X	X	X	X	X	X	X
60	0.35				X				
15	0.70	X	X	X	X	X	X	X	X

NOMENCLATURE

C_p	Static pressure coefficient, $(P - P_c)/q_c$
M_c	Equivalent plenum Mach number
$M_Q - M_c$	Tunnel calibration parameter
M_∞	Mach number
P	Static pressure, psfa
P_c	Plenum pressure, psfa
q_c	Equivalent plenum dynamic pressure, psf
$\Delta C_{p_{rms}}$	Root-mean-square fluctuating pressure coefficient, percent
$\Delta(C_p, \theta)$	Wall interference alleviation figure of merit [see Eq. (7)]
ΔM_Q	Flow uniformity figure of merit [see Eq. (1)]
ΔM_w	Wave cancellation figure of merit [see Eq. (2)]
θ	Flow angle, radians
λ	Tunnel pressure ratio
Φ	Nondimensional velocity potential
ϕ	Baffle angle, deg [see Fig. 3]

SUBSCRIPTS

Q_c	Centerline
c	Plenum
IF	Interference free
T	Tunnel
w	Wedge